Seizures and Quantitative EEG

4

Jennifer A. Kim, Lidia M.V.R. Moura, Craig Williamson, Edilberto Amorim, Sahar Zafar, Siddharth Biswal, and M.M. Brandon Westover

Introduction

Continuous EEG (cEEG) monitoring has become increasingly utilized as high rates of nonconvulsive seizures (NCS) and nonconvulsive status epilepticus (NCSE) in ICU patients have become widely recognized. Diagnosis of NCS and NCSE requires continuous EEG monitoring [1–3]. Timely seizure recognition is important as it may lead to acute changes in therapy aimed at suppressing seizures and correcting potential precipitating factors [4, 5].

As continuous EEG monitoring has become more prevalent, the time-consuming review necessary by neurophysiology experts trained in evaluating these records has become taxing and in many cases difficult to maintain. Although demand for continuous EEG (cEEG) monitoring has increased dramatically, the number of EEG readers has remained stable [6]. Many facilities that could benefit from the availability of cEEG may not have skilled EEG interpreters to provide ongoing interpretation of cEEG in the ICU. Even when skilled EEG reviewers are available, if multiple patients simultaneously undergo prolonged cEEG monitoring, interpretation and communication of findings becomes fragmented, the problem of "continuous monitoring and intermittent care" and delayed intervention [7].

J.A. Kim (✉) • Lidia M.V.R. Moura • E. Amorim • S. Zafar
S. Biswal • M.M.B. Westover
Department of Neurology, Harvard Medical School, Massachusetts General Hospital, Boston, MA 02114, USA
e-mail: jkim72@partners.org; lidia.moura@mgh.harvard.edu; EAMORIM@mgh.harvard.edu; SFZAFAR@mgh.harvard.edu; SBISWAL2@PARTNERS.ORG; MWESTOVER@mgh.harvard.edu

C. Williamson
Department of Neurology and Neurological Surgery, University of Michigan, University Hospital, Ann Arbor, MI 48109, USA
e-mail: craigaw@umich.edu

Routine evaluation of EEG consists of visual inspection of the data with an average review time of 20–30 min per 24-h study, with more detailed analysis taking more time [7]. Visual analysis of the raw EEG record may miss gradual trends in EEG that evolve over long periods of time [8]. To address these challenges, different quantitative methods to evaluate cEEG data have emerged. Advantages, hoped for, of quantitative EEG (qEEG) techniques include the ability to quantify information within the EEG signal, to compress the time scale and shorten the review time, to quickly identify events/periods of interest for closer analysis, and to make real-time monitoring more feasible. The main impetus for developing qEEG methods in ICU EEG has been to assist with rapidly identifying rare/occasional seizures in prolonged recordings without the need for exhaustive visual screening of each 10-s display window of raw EEG [9].

In summary, qEEG has the potential to improve efficiency of interpretation and communication in intensive medical care [10, 11]. However, qEEG remains a relatively new family of technologies, many of which are still in early stages of development, validation, and adoption. In this chapter we first provide a brief survey of qEEG methods that are in clinical use. We then provide a detailed treatment of one of the oldest and most clinically useful qEEG methods, "compressed spectral arrays" or spectrograms.

Overview of Quantitative EEG Methods

Amplitude-Based Methods

Amplitude-integrated EEG (aEEG) is a simplified bedside continuous EEG monitoring technology that has become widely used in the neonatal population over the past two decades to monitor for seizures and to assist with prognostication in neonates with hypoxic-ischemic encephalopathy [12]. aEEG is typically based on a limited number of

P.N. Varelas, J. Claassen (eds.), *Seizures in Critical Care*, Current Clinical Neurology, DOI 10.1007/978-3-319-49557-6_4

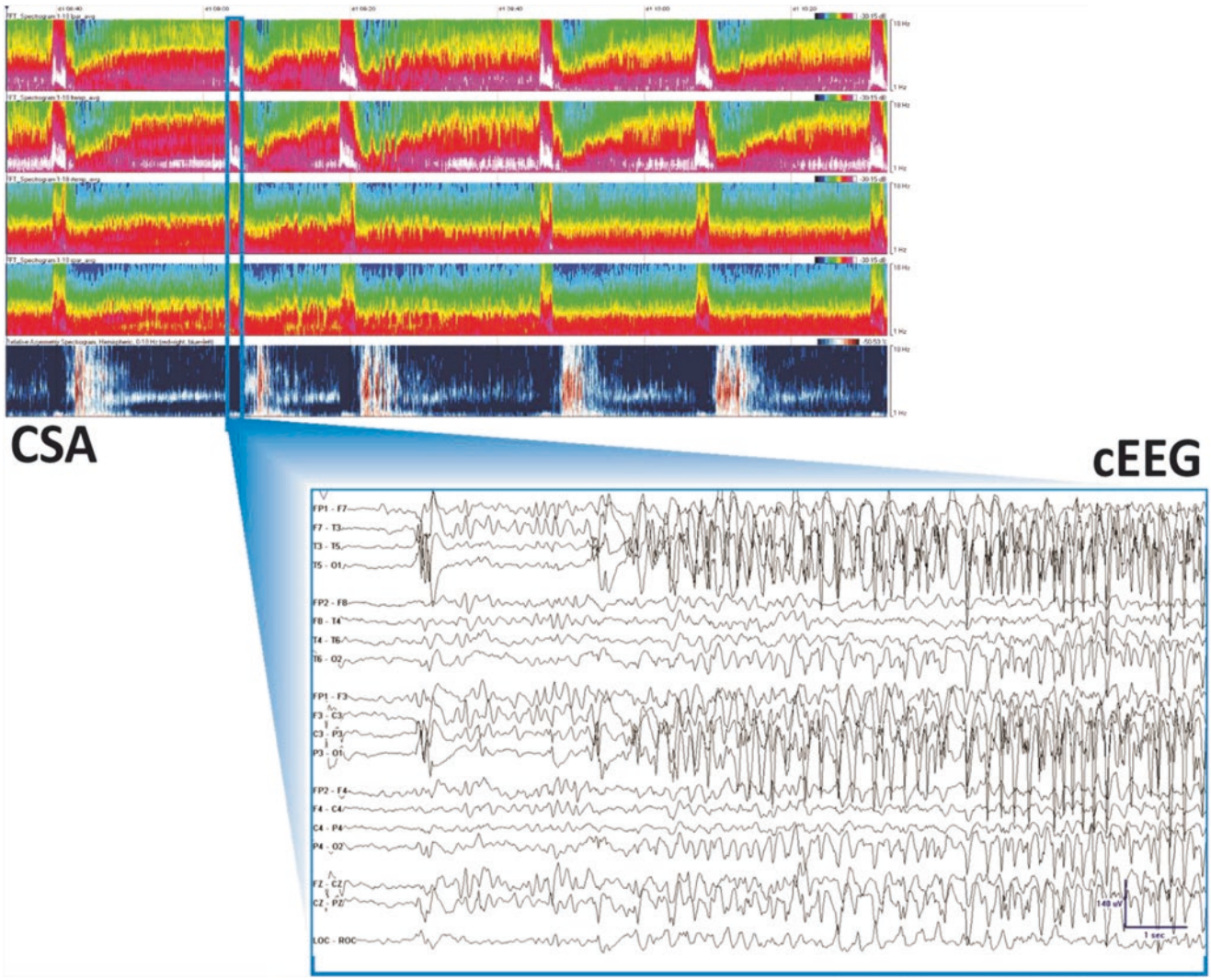

Fig. 4.1 An example compressed spectral array (CSA). Panels, *top to bottom*: left parietal average signal, left temporal average signal, right temporal average signal, right parietal average signal, relative asymmetry index. *Inset*: region CSA corresponding to the onset of a seizure as shown in the native EEG segment. This CSA is an example of *regular flame* pattern of seizures. Please see Sect. 5 and Table 4.1 for further details

recording channels, the data from which is filtered, rectified, and displayed on a semilogarithmic time- and amplitude-compressed scale [7]. Processed in this way, seizures are often evident as sudden increases and then decreases in EEG amplitude [13].

Envelope trend-based qEEG displays the median amplitude of all background activity over a specified time interval. Seizures can often be identified by an increase in median amplitude [9]. One study found that envelope trend analysis could accurately identify seizures lasting >1 min by experienced users with 88% sensitivity and few false positives [14].

Spectrograms

Various informative EEG displays may be created from the power spectrum as a function of time, also known as the compressed spectral array (CSA)) or spectrogram. By showing relatively large stretches of data in a compressed format while making changes in background activity salient, spectrograms can be used to expedite EEG review (Fig. 4.1) [10]. The spectrogram is sometimes referred to as the "FFT of the EEG," though this is a misnomer, as explained in the section on the theory of spectrograms.

Displays Derived from Spectrograms

Asymmetry trends use comparisons in power between homologous electrodes in the right and left hemispheres to highlight power asymmetries between the hemispheres. The comparison can be made based on absolute or relative power. This may be helpful to identify lateralized or focal seizures.

Asymmetry spectrograms are shown in subsequent sections as the fifth panel in the case examples discussed in section "Case Vignettes with Example Spectrogram Patterns". In our case examples, red represents greater power in the right hemisphere and blue represents greater power in the left hemisphere (though in other systems, this color scheme may be reversed).

Methods for Monitoring Burst Suppression

Monitoring burst suppression in ICU patients is another area in which qEEG can be informative. Pharmacologically induced burst suppression is often used in the treatment of refractory status epilepticus. In these cases EEG monitoring is important to ensure that medications can be appropriately titrated in real time to ensure appropriate levels of burst suppression while avoiding over- and under-dosing. It is also helpful to have such monitoring capabilities in patients with pathologically generated burst suppression patterns, such as after severe hypoxic-ischemic injury, to assess for trends in this background pattern for prognostication.

Burst suppression can be quantified using the burst suppression ratio (BSR), defined as the percentage of time within an epoch spent in suppression [15], or as the burst suppression probability (BSP), defined as the instantaneous probability that the EEG is in the suppressed state [15, 16]. Under steady-state conditions, the BSR and BSP agree closely. However, the BSP algorithm is better suited for tracking the depth of burst suppression under dynamic conditions. An example of tracking the BSP in a patient with status epilepticus is shown in Fig. 4.2.

Automated Seizure Detection

One of the ultimate goals of qEEG is to offer the potential for automated detection of clinically significant events such as seizures and ischemia. Ictal patterns are highly variable and thus make the development of such detectors difficult. Features that have been used to develop seizure detectors include amplitude, frequency, rhythmicity, and degree of asymmetry [9]. Most of these algorithms have been designed for identification of classic seizure patterns in the setting of the epilepsy monitoring unit. However, seizures in ICU patients typically have different characteristics than those of the EMU population and thus are not as reliably detected with standard seizure detection algorithms [9]. Pitfalls in qEEG analysis include the high degree of false-positive detections due to common ICU artifacts in addition to false negatives from very brief, low amplitude of slowly evolving seizures. Because seizures occurring in critically ill patients frequently exhibit patterns of rhythmicity and evolution that are slower than those seen in epileptic patients, existing detection programs may be relatively insensitive to certain types of ICU ictal patterns [8]. Another challenge is that many ICU seizures tend to wax and wane with subtle onset and termination rather than the abrupt ictal onset and cessation patterns of seizures typically seen in the EMU.

Automated Detection of Other Epileptiform Patterns

Recently one group has developed software, called NeuroTrend, that attempts to detect patterns in the long-term scalp EEGs in the ICU using the standardized EEG

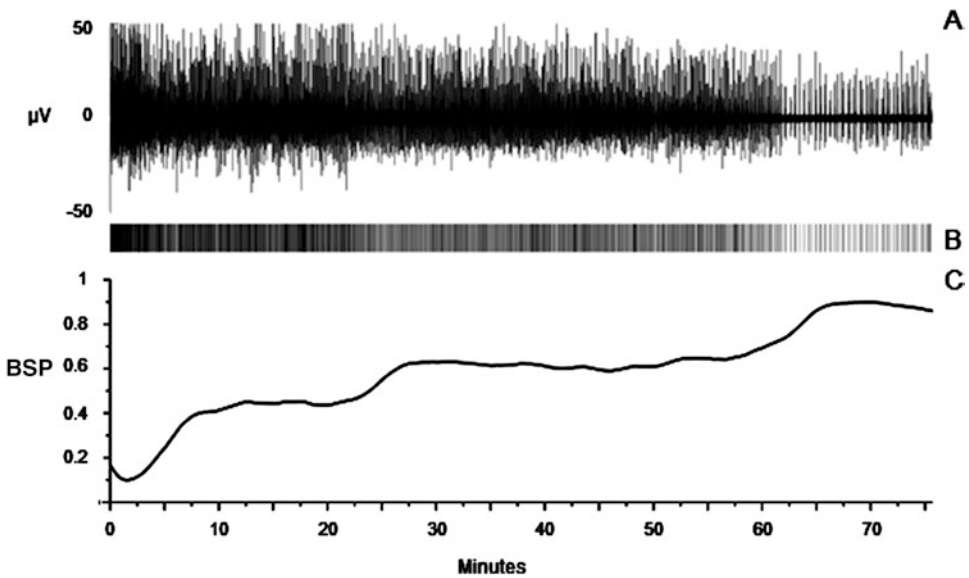

Fig. 4.2 Burst suppression probability (BSP)). (**a**) EEG signal compressed over 75 min. (**b**) Ticker plot representing each burst. (**c**) BSP increases over time as the periods of suppression become more frequent as the recording progresses

terminology [17]. Persyst Corp. has also recently developed an algorithm for identifying periodic discharges, available in version P13 of its software. Details from the algorithms from both NeuroTrend and Persyst Corp. are unpublished and proprietary. Rigorous external validation studies remain to be performed.

Fundamentals of Spectrograms

Motivation for Spectral Analysis

It is often natural to describe oscillatory signals like the EEG in the frequency domain. Indeed, this is reflected in the convention of describing clinical EEG recordings in terms of activity within frequency bands (e.g., delta, theta, alpha, and beta). In this section we briefly review key concepts from the mathematical analysis of frequency domain or spectral characteristics of signals. This overview will help the reader to better understand common features of spectrograms encountered in the ICU setting, reviewed in section "Interpretation of Spectrograms."

Spectral Decomposition: Fourier Transforms and the "FFT"

The basic problem of spectral estimation theory is: given a finite segment of a signal, *estimate* how the total power in the signal is distributed over a range of frequencies. The emphasis on estimation is because the EEG, like many other biological signals, is best regarded as composed of signal and noise. The noise must be suppressed in some way to obtain a clear view of the underlying spectral EEG characteristics that are of interest.

Before one can understand how to analyze stochastic signals like the EEG, one first needs to understand the principles underlying the more basic theory of spectral decomposition, which we will review now. Figure 4.3 shows the decomposition of a fairly complex 9-s long single-channel EEG signal into a series of sinusoids of varying phases and amplitudes. The black curve in Fig. 4.3a shows the original signal, consisting initially of a low-amplitude "baseline" period and an epileptiform discharge around $t = 4$ s, followed by a larger amplitude oscillating pattern at approximately 2 Hz that decays in amplitude while slowing in frequency to approximately 1 Hz by the end of the figure window.

The overlaid red curve is an approximation to the black curve, obtained by adding together a series of 50 sine and cosine waves or "components," with frequencies ranging from 0 to 35 Hz spaced evenly at intervals of approximately 0.7 Hz. The nine components which make the largest contribution to the approximation, i.e., the components with the largest amplitudes, sorted by frequency, are displayed in Fig. 4.3b.

For the most part, the sum of these sinusoidal components faithfully represents the original black signal. Careful scrutiny reveals that the approximation succeeds by a delicate series of constructive and destructive interferences of peaks and troughs. This remarkable balancing act is accomplished automatically by a mathematical formula known as the discrete Fourier series. In the examples shown in Figs. 4.3 and 4.4, the formula used is called the discrete Fourier transform, or DFT.

The amplitude spectrum for a signal is obtained by taking the geometric mean of the amplitudes of the sine-cosine pair for each frequency and plotting these amplitudes as a function of frequency, as shown in Fig. 4.3c.

For the most part, the red approximation or "reconstruction" is faithful to the original black signal. However, in places, the reconstruction is not accurate. These failures are instructive. Note particularly the epileptiform discharge or "spike" that occurs at approximately $t = 4$ s. Here, the reconstruction is smoother than the original signal. It fails to reproduce the abrupt rise in voltage and subsequent abrupt decrease that constitute the spike. This is because in this reconstruction we deliberately excluded sinusoids above 35 Hz from the reconstruction. The true bandwidth of the signal is evidently greater than 35 Hz. That is, higher frequency components are required in the Fourier sum to capture the more abrupt transitions or "sharper turns" that make up an epileptiform discharge. In this case, had we included components for all frequencies up to the Nyquist sampling rate (in this case, approximately 100 Hz), the reconstruction would have been essentially perfect.

Signal Sharpening Manifests as Amplitude Spectrum Broadening

We further illustrate the important relationship between "sharpness" and the presence of higher frequency components in the amplitude spectrum in Fig. 4.4. In Fig. 4.4a, we show a bell-shaped curve, reminiscent of an EEG "slow wave," together with the components in a frequency decomposition and the corresponding amplitude spectrum. As in the previous figure, there is an underlying black curve and an overlaid red curve which approximates the black curve as a sum of sinusoids with amplitudes calculated by the formula for the DFT. We see that, for a waveform with a blunted or non-sharp morphology, the amplitude spectrum is relatively narrow. By contrast, Fig. 4.4b shows a narrow, spikelike, bell-shaped curve, reminiscent of an epileptiform discharge. We see that a broader range of sinusoids extending to a much higher range of frequencies is required to faithfully represent

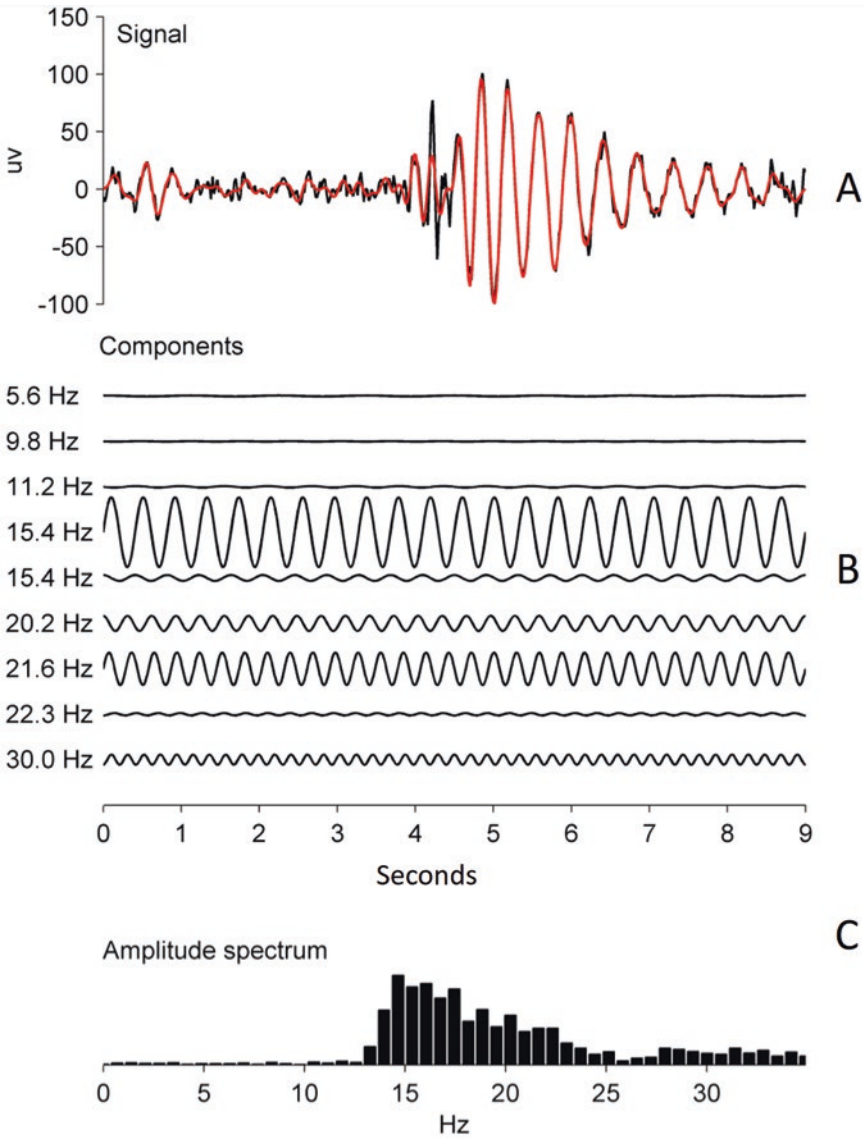

Fig. 4.3 Spectral decomposition. (**a**) Original signal (*black*) with superimposed approximation signal (*red*) composed of sine and cosine "components" making up the original signal. (**b**) Frequency decomposition—nine components which make up the largest contribution of the approximation. (**c**) Amplitude spectrum showing the distribution of frequencies contributing to the signal with higher amplitudes contributing more to the reconstructed signal

a spikelike transient. We will see that this observation, that signal "sharpness" manifests in the frequency domain as a broadening of the amplitude spectrum, is fundamental in interpreting spectrograms in ICU EEG monitoring.

From Spectra to Spectrograms

Though we have seen that it is possible to decompose complex signals into simple sinusoidal components, there is something unnatural about this decomposition for signals like the one shown in Fig. 4.3. In particular, the signal appears to change character over course of the 9 s shown. It would be more natural to break signals like this into smaller segments or windows, over which the signal characteristics are approximately constant. In statistical jargon, we desire to break the signal into segments that are statistically stationary.

Figure 4.5 shows an example of another signal that shows marked nonstationarity. This example shows a 3-min-long single-channel EEG signal. Figure 4.5b is the raw signal containing a seizure that begins around t = 20 s and ends around t = 120 s. The panels in Fig. 4.5a show the power spectrum (essentially, the amplitude spectrum squared, except for some smoothing—see next below) calculated from three different windows centered at t = 20, 60, and 130 s. The spectra within these three windows differ markedly, reflecting the evolution of signal characteristics that typify seizure activity.

Figure 4.5c shows the result of repeatedly calculating the spectrum of signals in 2-s windows, using a "sliding window" to obtain a new spectrum every 0.1 s. These spectra collectively form an image, or time-frequency spectrogram, formed by representing the power spectrum on a colormap. In this example, the power is shown in decibel (log) units,

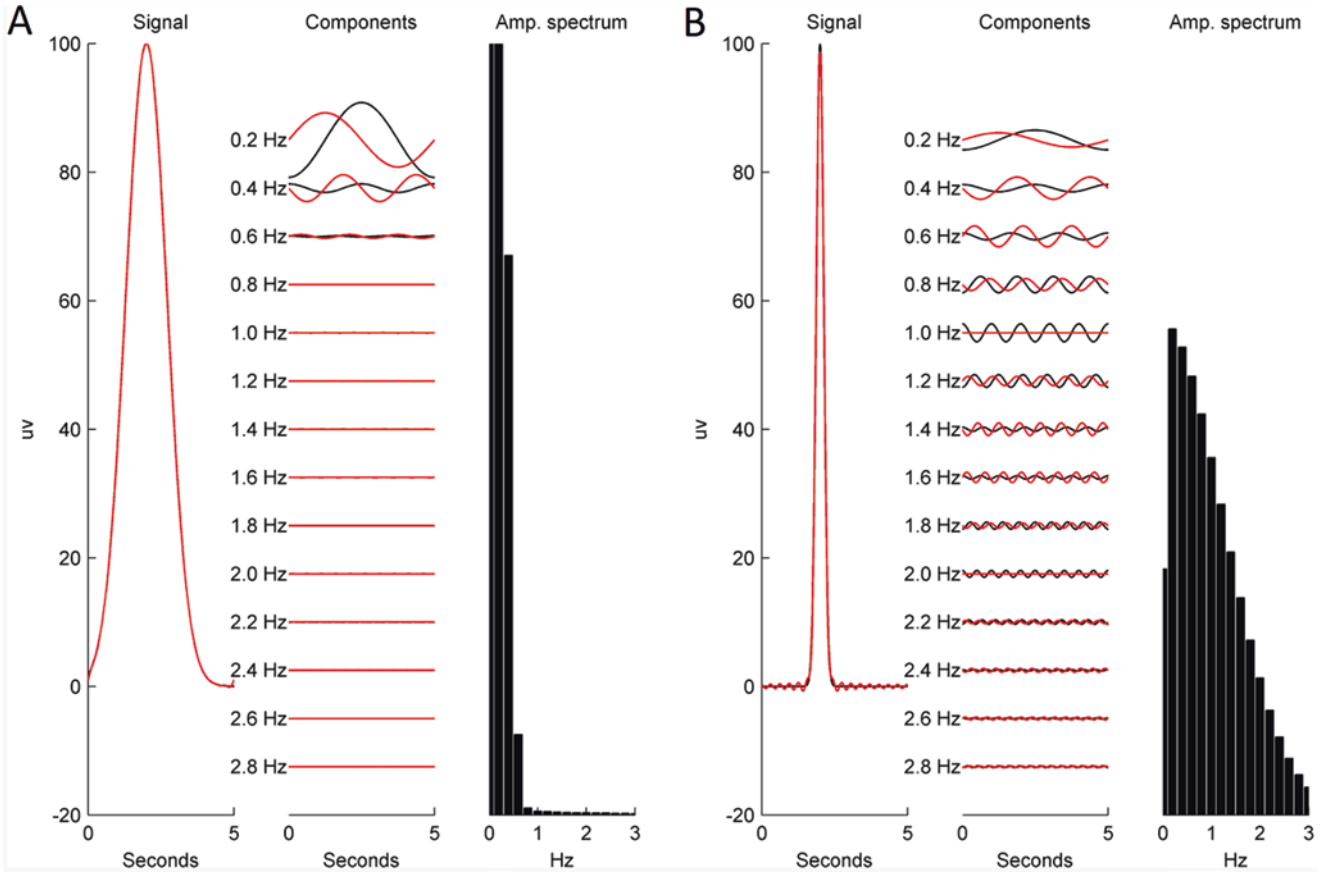

Fig. 4.4 Effect of signal "sharpness" on spectral components. (**a**) Bell-shaped "slow wave" with its frequency decomposition and amplitude spectrum. As with Fig. 4.3, the original signal (*black*) and approximation signal (*red*) are superimposed. Non-sharp morphology results in a narrow amplitude spectrum. (**b**) Narrow "spike-shaped" curve with the same functions plotted as in (**a**). This sharp morphology requires a broader range of sinusoids to approximate its signal

according to convention. This display convention allows simultaneous visualization of the signal power over a wide range of frequencies in one image, despite the fact that in human EEG the power at different physiologically relevant frequencies can vary by an order of magnitude or more. Representing this EEG signal as a spectrogram clearly brings out the salient dynamical features of the seizure, namely, an increase in the dominant frequency of oscillatory activity and a sharpening of the signal contour, followed by slowing down as the seizure ends. These features are not visible in the raw signal at this scale, though they are clearly evident when examining the signal within a more conventional 10-s window used for clinical review of EEG data. By contrast, these dynamics are clearly evident in the spectrogram despite the "large" 3-min window. The ability of spectrograms to display salient features of the EEG at a zoomed out or "compressed" scale is a major reason that spectrograms are useful in ICU EEG. Further examples at more compressed scales (2 h) will be discussed in subsequent sections.

Understanding Spectrograms: Cardinal Patterns from Synthetic Signals

The principles of spectral analysis described above are exploited to interpret patterns that occur commonly in spectrograms from cEEG recordings in the ICU setting. We illustrate these patterns using synthetic data in Fig. 4.5, before turning to real examples. Figure 4.6a shows a simple signal, a "monotonous" or unchanging low-amplitude sinusoid of 2 Hz. The corresponding spectrogram has a single peak at 2 Hz within every time window that manifests in the spectrogram as a red line at 2 Hz. This signal is reminiscent of the common ICU EEG pattern of "delta slowing" seen in patients with encephalopathy. Figure 4.6b shows a sinusoidal signal with a frequency that begins at 2 Hz, then increases following a linear ramp to 5 Hz while increasing also in amplitude, and then drops abruptly back to 2 Hz. The evolving portion of this pattern is manifest in the spectrogram as an upsloping line. This example is reminiscent of the classic pattern of

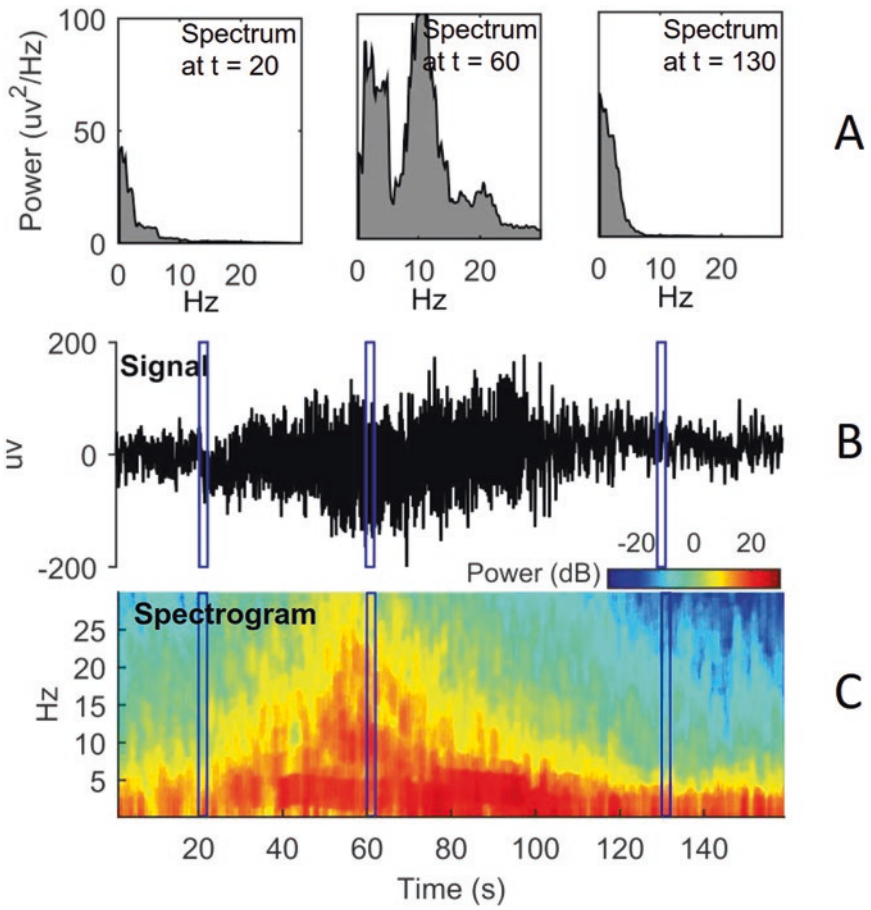

Fig. 4.5 Nonstationarity of a 3-min EEG signal containing a seizure. (**a**) Power spectra calculated at three different time windows of the recording (t = 20, 60, 130 s). (**b**) Raw EEG signal compressed over a 3-min interval, with *box insets* corresponding to the time windows plotted in (**a**). (**c**) Spectrogram of EEG signal from (**b**) using two sliding windows, box insets correspond to the time windows plotted in (**a**)

evolution characteristic of many epileptic seizures and typifies what we will refer to in a subsequent section as a "flame"-type seizure.

Figure 4.6c shows a more complex synthetic signal, consisting of a series of sharp discharges of randomly varying amplitudes, occurring in a regular or periodic fashion at 1 Hz. The spectrogram in this case shows high power not only at 1 Hz, reflecting the periodicity of the repeating pattern, but also a broadening of the spectrum up to approximately 5 Hz and beyond. This broadband character of the spectrogram reflects the fact that the morphology of the discharges is sharp and thus has a broad amplitude or power spectrum, as discussed previously in connection with Fig. 4.4b. Figure 4.6d shows another more extreme example, a sawtooth wave.

In both Fig. 4.6c, d, the pattern can be characterized as *broadband monotonous*, referring to the repetitive periodic nature combined with the relatively broadband of high power due to the sharpness of the underlying discharges. As will be seen in the real examples below, the *broadband-monotonous* pattern typifies the spectrogram when the underlying EEG is in a state of either periodic epileptiform discharges or certain closely related states of status epilepticus.

Technical Considerations: Trade-Offs in Spectral Estimation

Our discussion regarding spectral estimation has glossed over many important technical details that are critical in certain applications of spectral estimation. We touch briefly on two important fundamental issues that affect the quality of spectrograms.

Trade-Off Between Temporal and Spectral Resolution

Consider again the example of a seizure and its spectrogram shown in Fig. 4.5. In that example we chose to make the window size 2 s. This choice in turn dictated a limit to the level of detail with which we were able to resolve temporal features in the EEG, so that the spectrogram has a certain degree of blurring or smoothness across time. If we attempt to obtain higher temporal resolution by making the analysis windows progressively smaller, we would at the same time see that we progressively lose the ability to distinguish detail in the frequency domain. This is because decreasing the signal

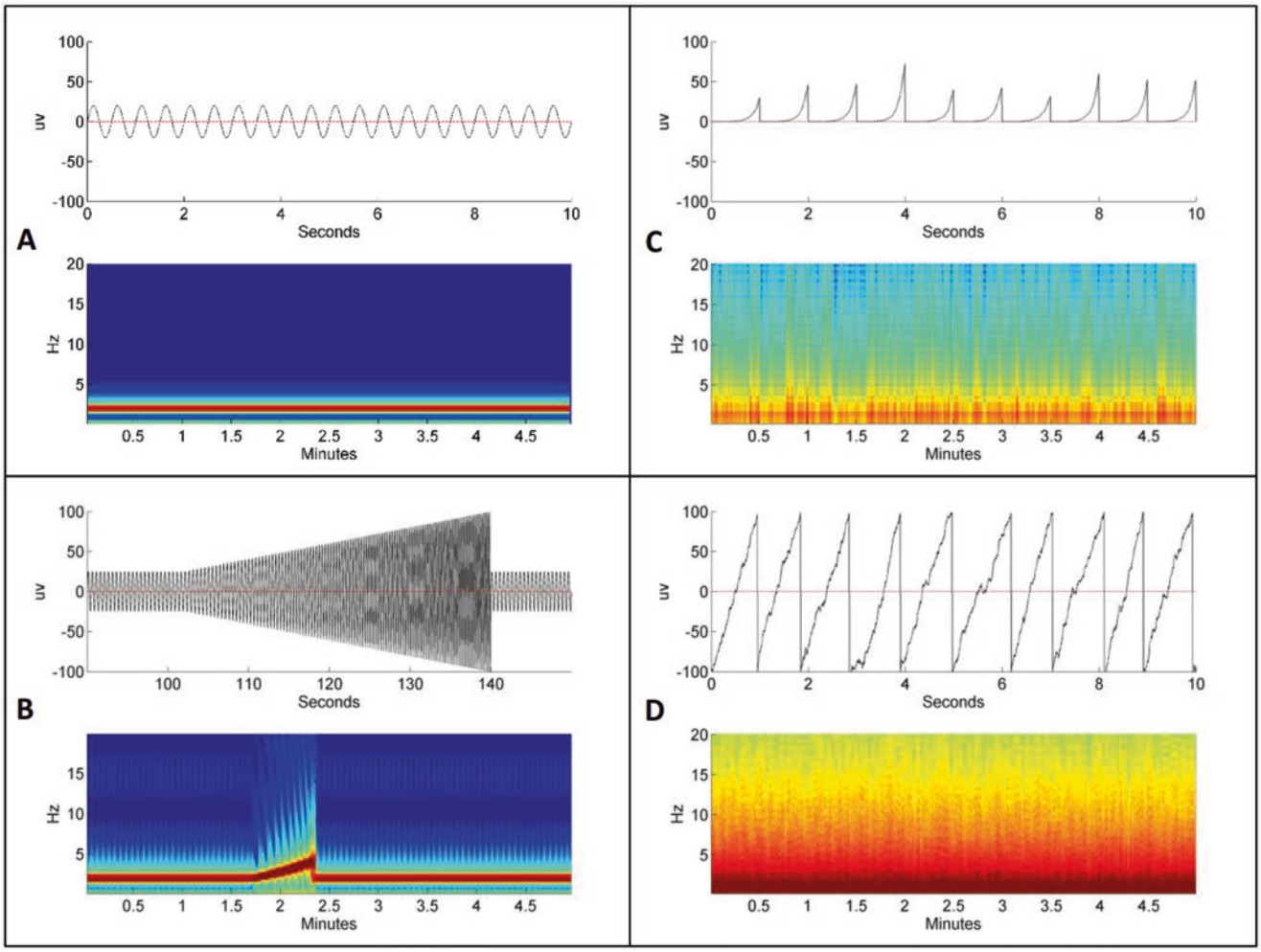

Fig. 4.6 Four simulated EEG patterns converted to CSAs. (**a**) Sinusoidal signal at 2 Hz without variation, reminiscent of "delta slowing." CSA shows a *red line*, representing a consistent peak at 2 Hz. (**b**) Sinusoidal signal with linear ramp from 2 to 5 Hz followed by an abrupt termination, modeling an evolving seizure. CSA shows a rise in the power of frequencies up to 5 Hz corresponding to the linear ramp seen in the sinusoidal signal and a return back to 2 Hz. (**c**) Synthetic model of periodic sharp discharges at 1 Hz. CSA shows a high-power band at 1 Hz with a broadening of the spectrogram reflecting the sharpness of the discharges as described in Fig. 4.4. (**d**) Synthetic model of extreme sawtooth pattern, which best exemplifies the *broadband-monotonous* pattern described in Table 4.1

segment length (keeping the sampling rate constant) reduces the number of frequency components and increases the spacing between components in the DFT. In effect, nearby peaks in the spectrum become single peaks, in the same way that creating a histogram using wide bins can smooth together and obscure peaks in a distribution that has multiple modes.

This consideration highlights a fundamental trade-off that exists between the maximal spectral resolution (the level of detail with which we can calculate the spectrum, i.e., the spacing between frequency components) and the maximal temporal resolution (the smallest window over which we can perform spectral analysis on a signal). The mathematical reasons behind the trade-off between temporal and spectral resolution are in fact identical to those that describe the well-known "Heisenberg uncertainty principle," which describes the inverse relationship between the precision with which one can simultaneously measure the position and velocity of a particle.

Trade-Off Between Bias and Variance

A second fundamental trade-off arises from the fact that the EEG, like many other naturally occurring signals, is best regarded as stochastic, containing an underlying signal of interest that is corrupted by noise. Consequently, the spectrum and hence the spectrogram need to be estimated. This fact gives rise to a trade-off between bias and variance.

The bias-variance trade-off in spectral estimation is illustrated in Fig. 4.7. In Fig. 4.7a, we show a sample of a stochastic signal generated by a model with a known power spectrum, shown as a red curve in Fig. 4.7b–e. This spectrum has two peaks, at approximately 11 and 14 Hz. Let us assume that we have already chosen a window size for our spectral estimates, based on either the maximum window length over which the signal can be considered to be statistically station-

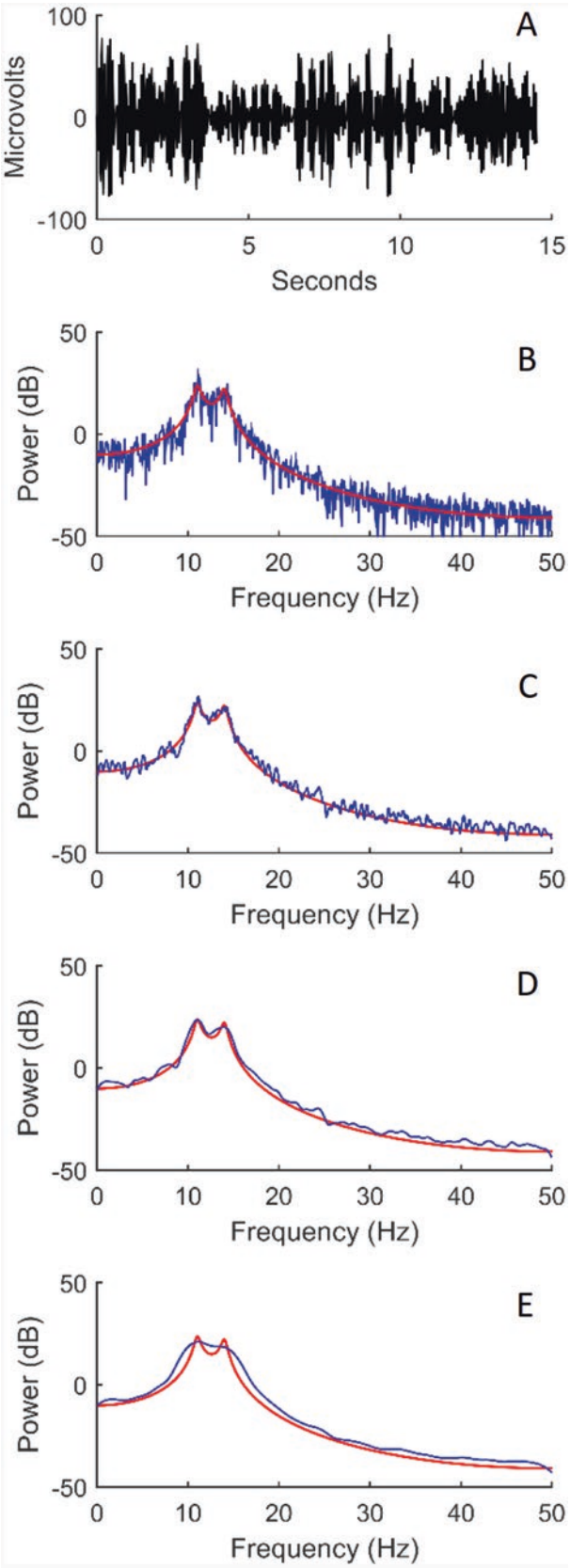

Fig. 4.7 The bias-variance trade-off. (**a**) A stochastic signal generated by a model with a known power spectrum (*red curves*, **b**–**e**). (**b**–**e**) Test of varying time windows used for estimating the discrete Fourier transform. Short time windows (**b**) result in noisy estimations, while broad windows (**e**) smooth the data so much as to make peaks indistinguishable

ary or the desired level of temporal resolution. In this case we have chosen a window size of 15 s.

Given the chosen window length, a common but suboptimal way to obtain a spectral "estimate" from this finite-length signal is simply to calculate the discrete Fourier transform, usually using a fast algorithm known as the "fast Fourier transform" (FFT), and to then take the squared amplitude of the result as an estimate of the power spectrum. The result is shown as the blue line in Fig. 4.7b. The spectrum appears very noisy. This is not surprising when one considers that what we have done amounts to "estimating" a quantity using only a single sample. Estimates obtained in this way are sometimes called "periodograms." (We have passed over the fact that, technically, to calculate the periodogram, one usually multiplies the signal by a windowing function or "data taper" before computing the FFT to reduce an effect known as spectral leakage. All spectral estimates shown in this chapter have been computed with appropriate data tapers.)

Under the right conditions in a laboratory, it might be possible to obtain numerous repeated sample segments of the same signal. Given enough repeated samples, we could obtain an accurate estimate of the underlying true spectrum by averaging periodograms. However, in ICU EEG monitoring, we of course do not have the luxury of holding the patient's state constant to obtain repeated samples. We are thus forced to resort to methods of reducing the variance of the spectral estimates, i.e., of making the spectrogram smoother. Figure 4.7c–e show progressively more aggressive smoothing of the original signal. Smoothing necessarily blurs together fine spectral details, as evidenced by the fact that beyond a certain point the spectral peaks in this example become indistinguishable (Fig. 4.7e).

We operationally define the spectral resolution of the estimated power spectrum as the minimum distinguishable difference between two narrow peaks that can be distinguished in the estimated spectrum. Judging by eye, the approximate spectral resolution in Fig. 4.7c–e is <1 Hz, 2 Hz, and 5 Hz, respectively. The optimal trade-off between variance reduction (smoothness) and spectral resolution in this example appears to be most closely achieved in Fig. 4.6d. Note that the spectral resolution is thus usually lower than the maximal spectral resolution discussed in the preceding subjection. The maximal spectral resolution depended on the window width rather than on statistical considerations.

The most appropriate degree of spectral smoothing clearly depends on the spectral characteristics and intrinsic smoothness of the underlying processes which generate the signal and thus varies depending on the application. In clinical ICU EEG monitoring, a spectral resolution of approximately 0.75 Hz is usually adequate and allows for sufficient spectral smoothing to obtain high-quality spectral estimates. This is the resolution used for the spectrogram in Fig. 4.5 and in the examples shown later.

Numerous approaches to spectral smoothing have been proposed. Common methods include averaging spectra from consecutive neighboring windows ("weighted overlapping segment averaging," WOSA) or replacing the amplitudes in a "noisy" spectrum obtained from an appropriately computed discrete Fourier transform by locally weighted averages of neighboring values. Various window functions or "kernels" can be used for this "kernel smoothing" method. The current state of the art, however, is the method called multitaper spectral estimation algorithm (MTSA), which involves averaging together the amplitude spectra of multiple discrete Fourier-transformed segments that have been pre-multiplied by a specific series of windowing functions or "tapers," known as the discrete prolate spheroidal sequences (DPSS). While the technical details of MTSA are beyond the score of this chapter, it suffices for our purposes to know that MTSA is the solution to a mathematically well-defined optimization problem, designed to achieve a balance between spectral resolution (bias) and the variance of spectral estimates. Surprisingly, though it was invented in the early 1980s, MTSA is not yet in wide use. In fact spectral estimation routines implemented in many commercial products produce relatively poor-quality spectrograms, very often simply "computing the FFT" [18–20].

As with all smoothing methods, MTSA has adjustable parameters that allow one to decide precisely how to balance the bias against variance. In the remaining figures shown in this chapter, spectrograms are computed with a moving window length of 4 s, with overlapping windows shifting by 0.1 s, and a spectral resolution of 0.75 Hz.

Interpretation of Spectrograms

We now turn from theory to the interpretation of ICU EEG recordings. While there is no single pattern on a spectrogram that is invariably associated with seizures or other abnormal periodic patterns, many events of interest fall into a small number of recognizable patterns. In this section we briefly review some of the most common spectral patterns associated with pathological ICU EEG events. In the next section, we review a series of actual cases to gain experience with spectrogram interpretation.

The most easily recognizable seizures present with an abrupt increase in power across a range of frequencies that stands out clearly from the surrounding background. Given the red and white color typically used to indicate high power on a color density spectrogram and the shape of these events in the spectrogram, these abrupt changes resemble small flames (e.g., Fig. 4.1). We refer to this pattern as *regular flame*, to distinguish it from the less clear-cut pattern of *choppy flame* (see below).

Cyclic seizures are also often easy to recognize as a series of repeating *regular flame* events (e.g., Figs. 4.1, 4.8, and 4.9).

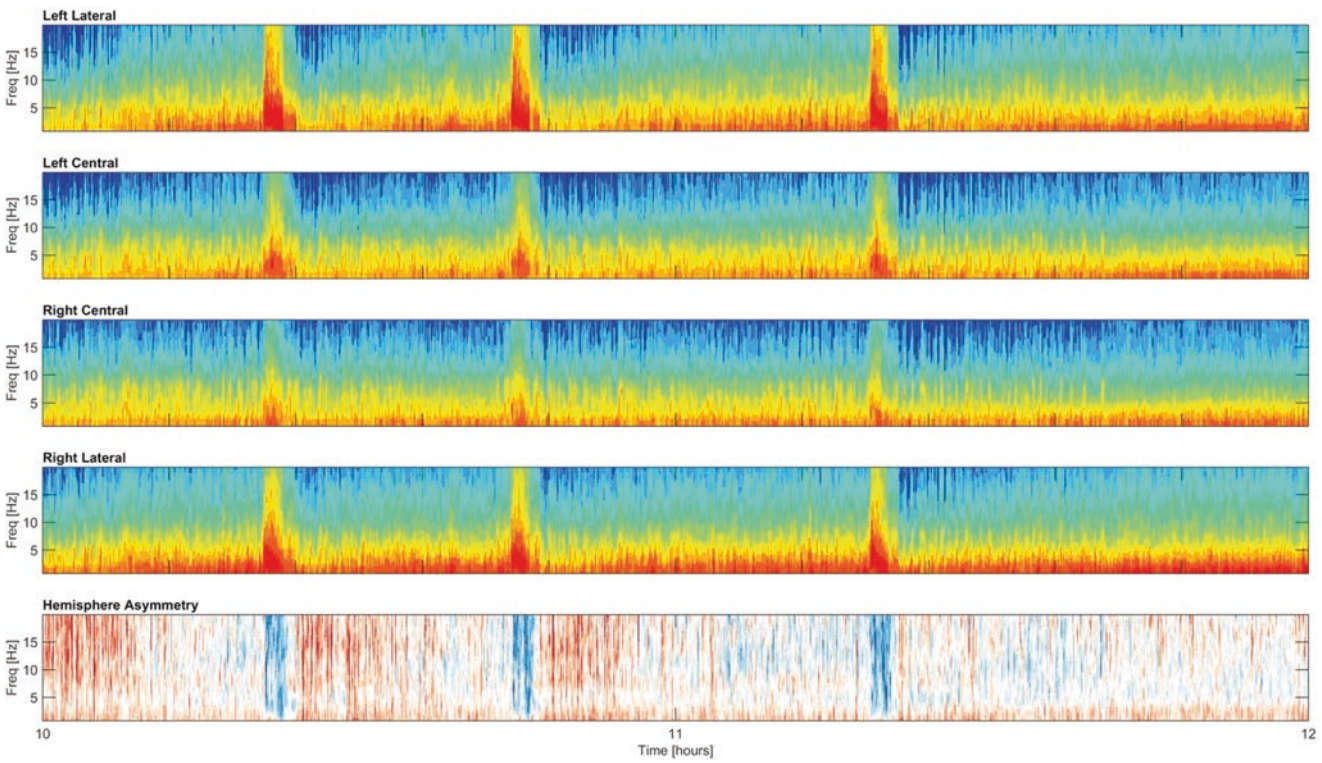

Fig. 4.8 Cyclic seizures (Case 1). This example is typical of the *regular flame* morphology. For Figs. 4.8–4.23, the 2-h CSA panels are displayed as follows (from top): left lateral, left central, right central, right lateral, and hemisphere asymmetry (a.k.a. relative asymmetry). For the top four panels, high power is in *red* and low power in deep *blue*. The hemisphere asymmetry panel assesses where spectral power of the right > left hemisphere (*red*), left > right hemisphere (*blue*), or both are equal (*white*)

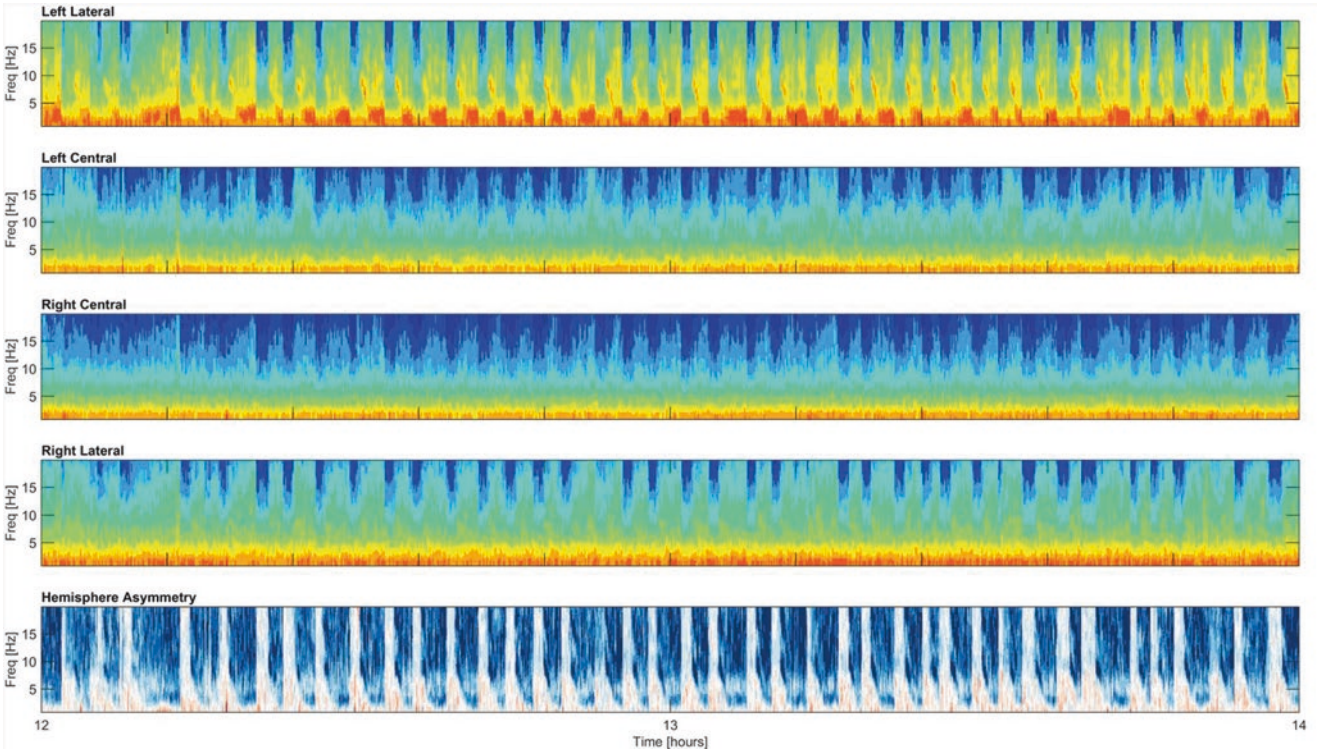

Fig. 4.9 Frequent cyclic seizures (Case 2). Again, this shows the *regular flame* morphology

Once a cyclic seizure has been verified by review of the raw EEG, further seizures can often easily be identified by review of the spectrogram alone. It may even be possible for inexperienced users at the bedside, such as nurses or residents, to detect recurrent seizures in these cases.

State changes and decreased sedation may also cause relatively abrupt increases in power that may mimic flame-type seizure patterns. However, these changes will often have a choppier or more irregular appearance than when an actual seizure is present; hence we refer to these as *choppy flames* (e.g., Fig. 4.10). However, in practice, differentiating seizures from other changes without review of the raw EEG can be challenging.

Similarly, longer-lasting nonconvulsive seizures or periodic discharges often manifest with a spectral signature that is high power across a broadband of frequencies, extending from delta up to theta or higher. These patterns are often unchanging or "monotonous" over long periods or exhibit only changes in their spectral signatures, without a clear beginning or end. We refer to these patterns as "broadband monotonous." The broadband-monotonous patterns are high power because of their typically high amplitude. They are broadband because of the regularity and sharpness of the underlying waveforms, as was explained in the synthetic examples shown in Fig. 4.6c, d. Other examples are shown in the cases that follow (e.g., Figs. 4.11 and 4.12).

As opposed to the broadband-monotonous pattern, diffuse nonrhythmic slowing as is commonly seen in patients with encephalopathy who are not having seizures typically produces a spectral pattern that is monotonous and relatively restricted to the low-frequency part of the power spectrum. We refer to this pattern as "narrowband monotonous" (e.g., Fig. 4.18).

A final easily recognizable common spectral pattern in ICU EEG is that of burst suppression. Burst suppression typically appears as a series of colored "stripes," representing the bursts, alternating with a blue (low-power) background, corresponding to the suppression periods (e.g., Fig. 4.14).

Very brief or very focal seizures may be missed by spectrogram review alone [10, 11]. Because spectrograms compress EEG data and display long periods of time on a single screen, very brief seizures may not result in an identifiable change. Similarly, as spectrograms typically average across a number of leads, very focal seizures may also be impossible to visualize.

Case Vignettes with Example Spectrogram Patterns

In this section, we show several examples of common patterns encountered in EEG spectrograms of ICU patients, including seizures, periodic discharges, and artifact. Where possible, we will describe these patterns using the categories introduced above: *regular flame*, *choppy flame*, *broadband*

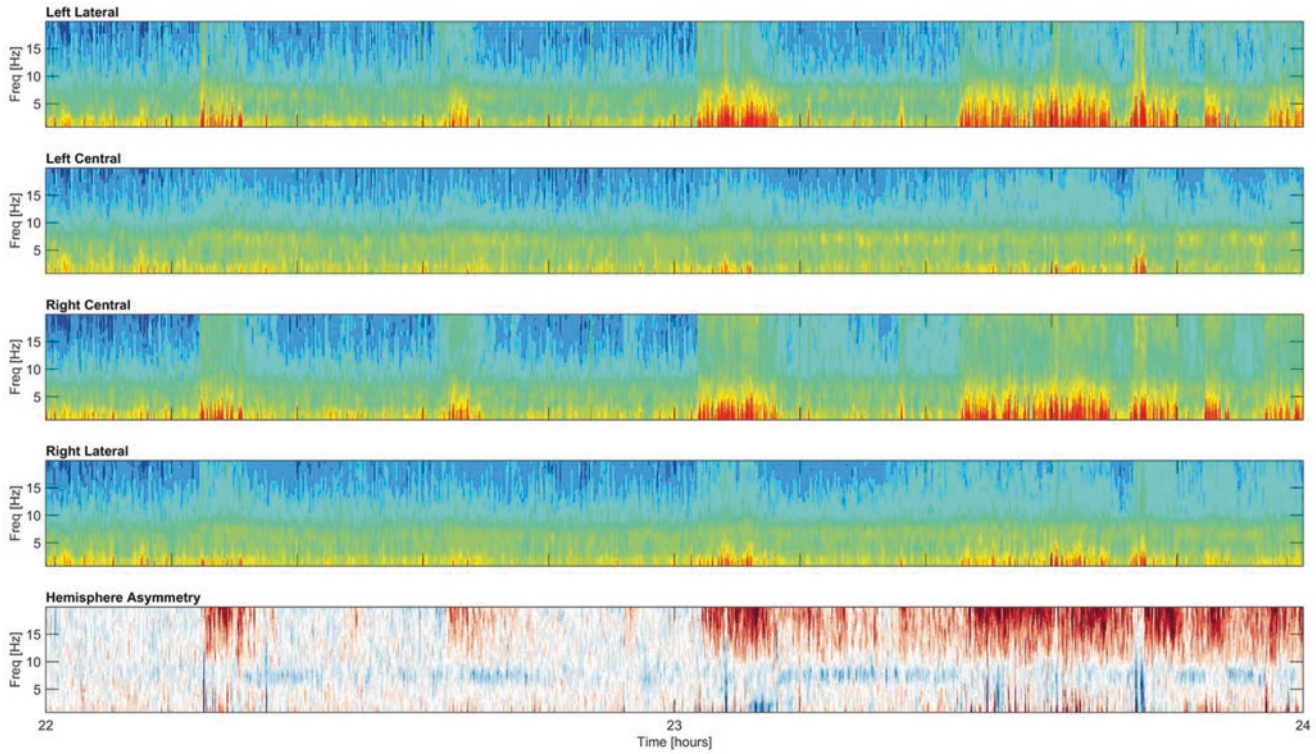

Fig. 4.10 *Irregular flame* morphology (Case 3). This pattern often represents seizures, but can correspond to waxing and waning periodic discharges or artifacts

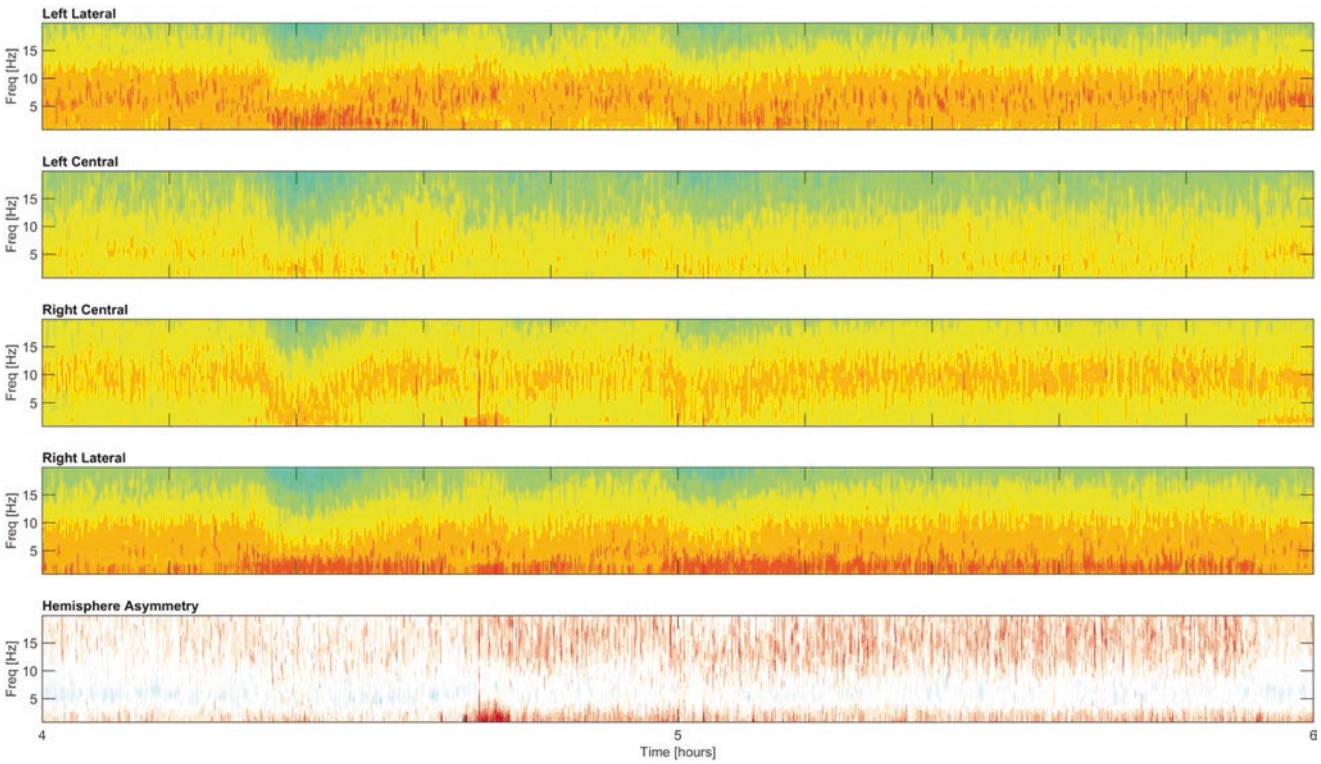

Fig. 4.11 Postanoxic status epilepticus (Case 4). A striking example of the *broadband-monotonous* pattern, often seen with status epilepticus or with periodic discharges

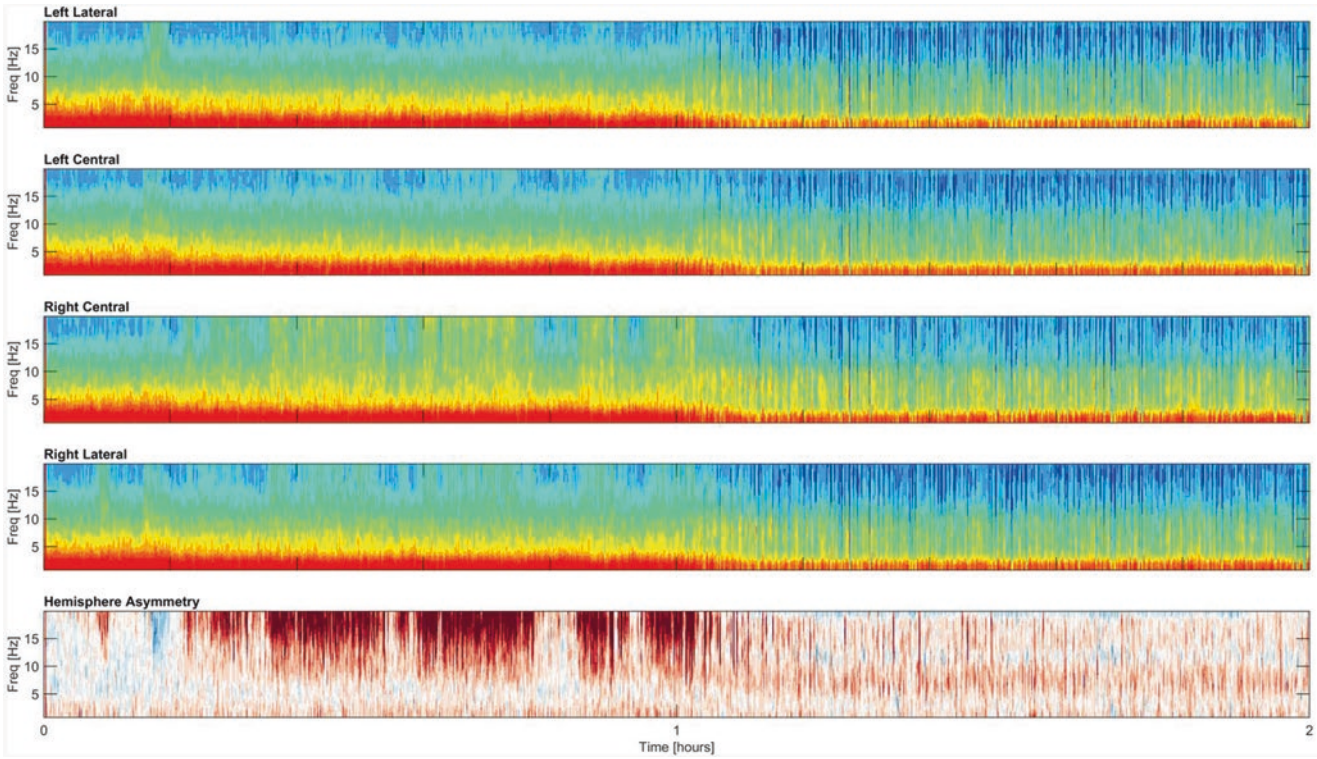

Fig. 4.12 Nonconvulsive status epilepticus (Case 5). A more typical example of the *broadband-monotonous* pattern

Table 4.1 Proposed nomenclature for common spectrographic patterns

Spectrogram pattern	Description	Example(s)
Regular flame	Sudden rise and subsequent fall in power across a broad range of frequencies in a brief period reminiscent of a candle flame This is the most common seizure pattern observed	Fig. 4.8 Fig. 4.9
Choppy flame	Discrete events that stand out against the background, but each event is not as well formed and solid as in the *regular flame* pattern. The flames are more "wispy" This most often reflects seizures, but can correspond to periodic discharges or artifacts	Fig. 4.10
Broadband monotonous	High-power band over a broad range of frequencies across time. Appears as a thick band across the spectrogram This is seen either in status epilepticus or with periodic discharges or less often in high-amplitude rhythmic delta activity	Fig. 4.11 Fig. 4.12
Narrowband monotonous	High-power band over a narrow range of frequencies across time. Appears as a thin band across the spectrogram This is most commonly seen in focal or generalized slowing	Fig. 4.13
Burst suppression	Repetitive dark blue vertical stripes, corresponding to "suppression segments," alternating with brighter (higher power) stripes representing high-power "bursts"	Fig. 4.14

monotonous, *narrowband monotonous*, and *burst suppression* (Table 4.1). We note that while the authors have found these terms helpful, they are not presently part of any officially recognized or validated nomenclature.

Basic Patterns

Case 1: (Fig. 4.8)

A 75-year-old woman with a history of dementia and anticoagulation for deep venous thrombosis presented with seizures in the setting of a left frontoparietal hemorrhage secondary to cerebral amyloid angiopathy. Her cEEG showed 3–5 electrographic nonconvulsive seizures per hour and left centrotemporal and posterior lateralized periodic discharges (LPDs).

In this spectrogram one sees three generalized electrographic seizures with clearly defined discrete starting and

ending points. This example is very similar to the example in Figs. 4.1 and 4.5. The sudden rise and subsequent fall in power across a broad range of frequencies in these discrete intervals is reminiscent of a candle flame. This is an example of the *regular flame* pattern characteristic of many seizures.

The background EEG between seizures showed generalized periodic epileptiform discharges. The corresponding spectrogram, not surprisingly, falls into the *broadband-monotonous* category (described in Cases 4 and 5), with prolonged periods lasting more than 10 min at a time of high-power activity extending above 5 Hz.

Case 2: (Fig. 4.9)

A 75-year-old man presented with a syncopal episode resulting in a left frontoparietal skull fracture and an underlying parenchymal contusion. His hospital course was complicated by intracranial hypertension and status epilepticus. The patient developed repetitive, regularly recurring left hemisphere seizures. Seizures started abruptly with 10–12-Hz low-amplitude (<20-mV) discharges and had no clinical correlate. A diagnosis of nonconvulsive status epilepticus was made.

The seizures in this example again fit into the category of *regular flame* seizures. The repetitive, periodic nature of these events demonstrates a spectrographic pattern of left hemisphere cyclic seizures.

The background in the right lateral, left central, and right central regions had a *narrowband-monotonous pattern* (described in Case 6), corresponding to diffuse slowing in these regions on the raw EEG.

Case 3: (Fig. 4.10)

A 70-year-old woman with a history of stroke, subarachnoid hemorrhage, and seizures presented with status epilepticus in the setting of bilateral subdural hematomas. After treatment with anticonvulsants, her cEEG revealed bilateral independent multifocal sharp waves and recurrent discrete nonconvulsive left centrotemporal seizures.

The seizures in this case have a different spectrographic thumbprint from the preceding cases. There are still discrete events that stand out against the background, but each event is not as well formed and solid as in the prior two cases. These "flames" are more "wispy," perhaps reminiscent of flames generated by an electric fireplace. We have termed this the *choppy flame* spectrographic pattern. While this pattern often reflects seizures as in this case, it can also correspond to waxing and waning periodic discharges or artifacts more often than the *regular flame* pattern.

Case 4: (Fig. 4.11)

A 36-year-old woman with a history of alcohol abuse presents with coma after cardiac arrest. Despite undergoing therapeutic hypothermia, she developed generalized periodic discharges at 5 Hz consistent with postanoxic nonconvulsive status epilepticus.

This is a striking example of a spectrogram where the power is relatively high over a broad range of frequencies, which changes slowly with time. In the spectrogram one sees a thick orange band going across the left hemisphere spectrogram and a lighter yellow band over the right hemisphere regions. The thickness of this band remains relatively stable across the displayed recording time, waxing and waning slowly. Given these features, this pattern can be described as *broadband monotonous*. This pattern can be seen with either status epilepticus (as in this case) or with periodic discharges, as discussed in connection with Fig. 4.6c, d.

Case 5: (Fig. 4.12)

A 50-year-old female with developmental delay, familial transthyretin amyloidosis, and non-aneurysmal subarachnoid hemorrhage presented with acute hydrocephalus. The patient had near continuous seizures that persisted until an intravenous propofol infusion was initiated.

This is a more typical example of the *broadband-monotonous* spectrogram pattern. The widening of the red stripe corresponds to increased power and sharpness and reflects in this case continuous nonconvulsive seizure activity. The power then shifts back to the lower frequencies as propofol is uptitrated. Near the end of the 2-h epoch, the EEG has entered a state of *burst suppression*, as reflected by the appearance of a striped pattern in the spectrogram (compare with Case 7, Fig. 4.14).

Case 6: (Fig. 4.13)

An 83-year-old man with a history of end-stage renal disease, coronary artery bypass grafts, hypertension, and hyperlipidemia presented with aphasia and poor mental status. He was found to have a left middle cerebral artery stroke. He had some intermittent staring spells, which were concerning for seizures, so cEEG monitoring was performed. His EEG showed diffuse slowing without any epileptiform abnormalities.

Here, one can appreciate a thin yellow-orange band that continues through the displayed record in the low (<3-Hz)-frequency range. Unlike the broadband-monotonous pattern, this *narrowband-monotonous pattern* is most commonly associated with focal or generalized slowing observed on cEEG, rather than periodic discharges or seizures.

Case 7: (Fig. 4.14)

A 33-year-old man with history of severe traumatic brain injury and meningitis status-post ventriculoperitoneal shunting presented with status epilepticus due to shunt malfunction. His EEG showed evidence of recurrent right frontotemporal 2–3-Hz sharp waves evolving to 3–4-Hz lateralized periodic discharges, unresponsive to second-line

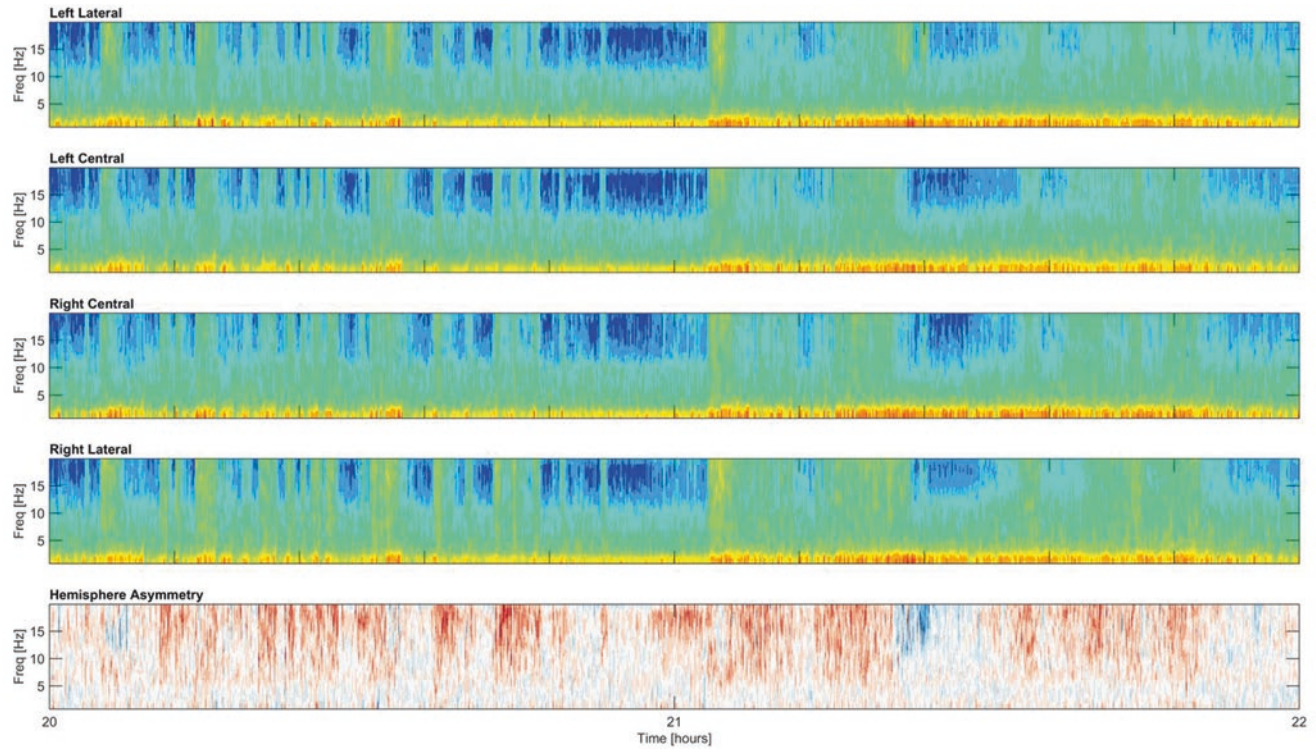

Fig. 4.13 Diffuse slowing (Case 6). This is an example of the *narrowband-monotonous* pattern, often seen in focal or diffuse slowing

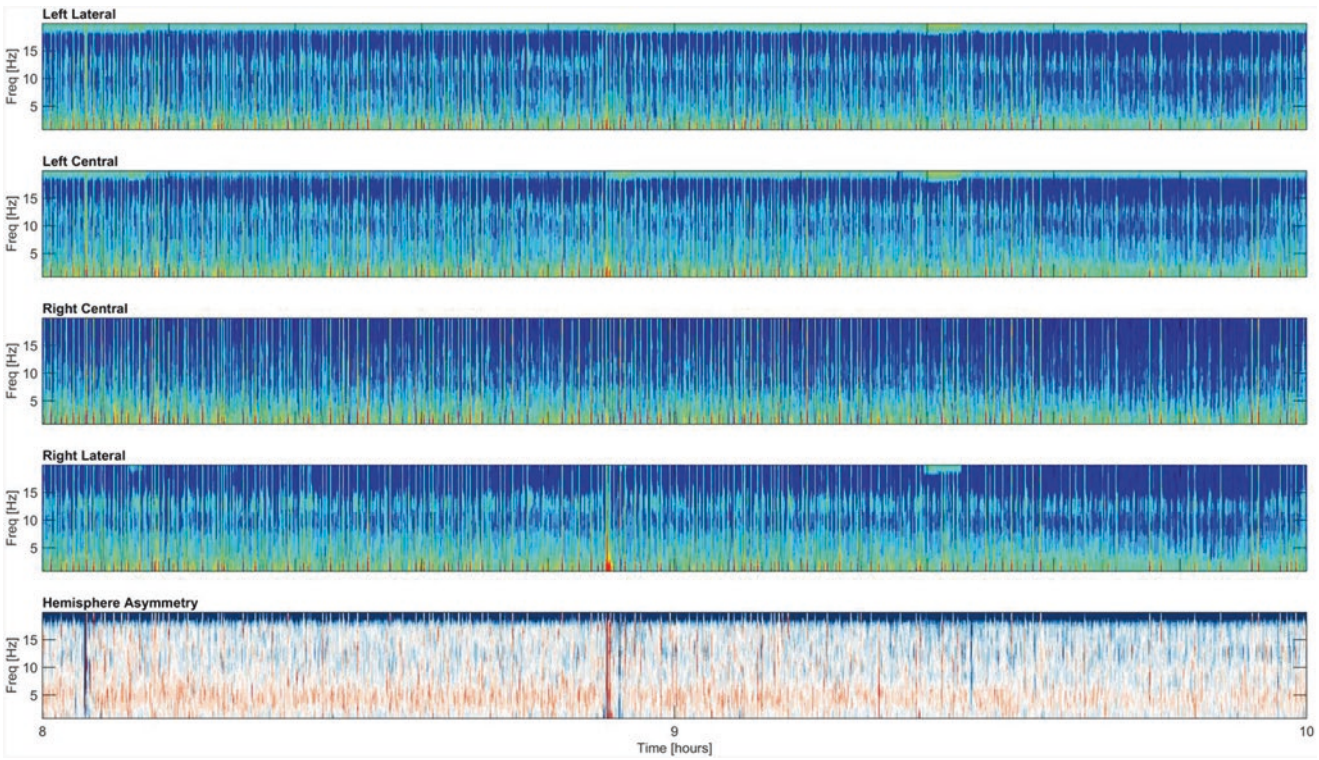

Fig. 4.14 Burst suppression on propofol and midazolam (Case 7). Here is an example of what *burst suppression* patterns look like on CSA

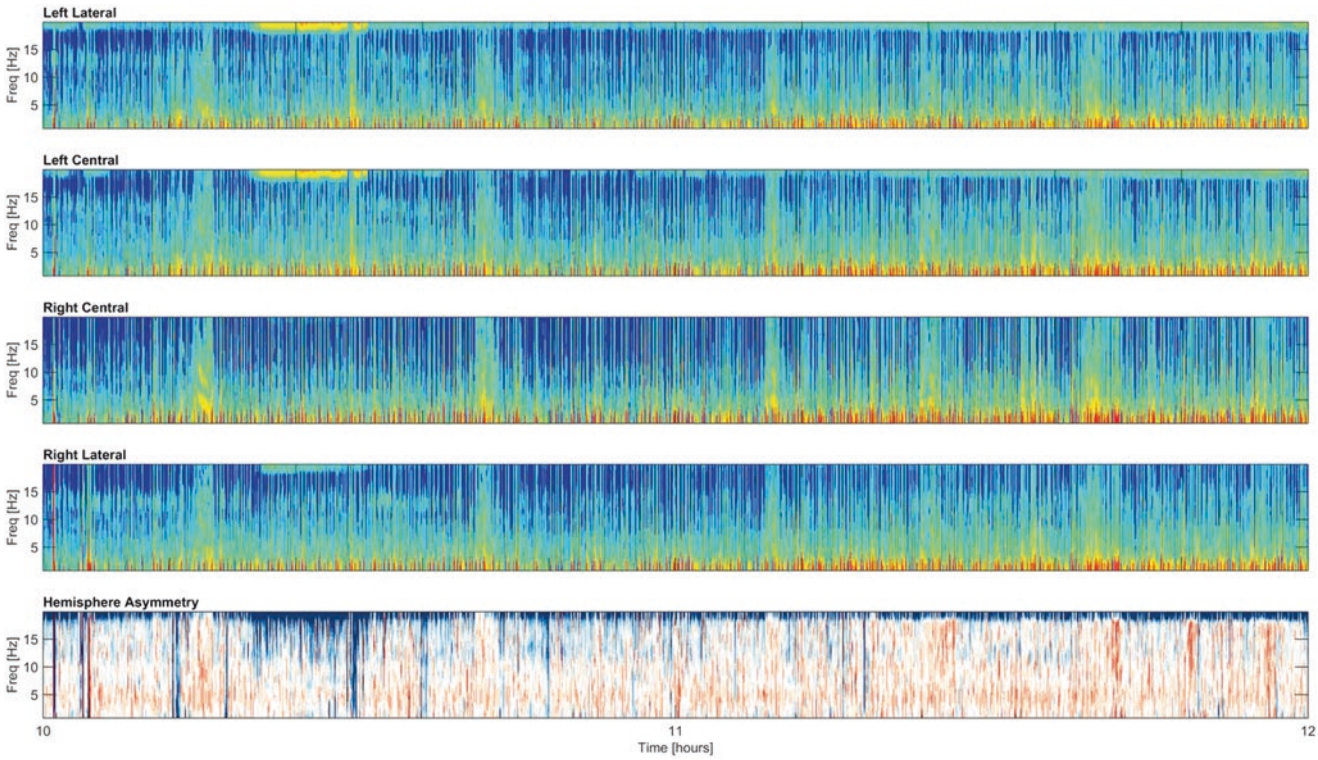

Fig. 4.15 Lifting sedation after burst suppression (Case 7, continued). Here is a continuation of the CSA in Fig. 4.14, showing the *burst suppression* pattern lightening and the emergence of *regular flame*-shaped seizures

intravenous anticonvulsants. He was diagnosed with refractory status epilepticus and treated with intravenous propofol and midazolam.

This is an example of a *burst suppression* on a spectrogram. There are repetitive dark blue vertical stripes throughout the record. The dark blue stripes correspond to the "suppression" segments and the light blue stripes with associated small red-orange bases represent the higher power "bursts."

Case 7, continued: (Fig. 4.15)

This is the succeeding epoch of the same case vignette above. Here, one can again appreciate dark and light blue stripes representing the signature pattern for *burst suppression*. However, during this displayed epoch, sedation was lightened. As *burst suppression* lightens, one can appreciate that the density of the dark blue stripes lessens. One can also appreciate the emergence of at least four *regular flame*-shaped seizures "breaking through" as sedation lightens.

Combination Patterns

Case 8: (Figs. 4.16–4.18)

An 83-year-old man with a medical history significant for chronic kidney disease and atrial fibrillation developed status epilepticus after cardiac arrest. The cEEG showed diffuse background attenuation associated with generalized periodic discharges and myoclonic movements. Sedation was increased and the seizures resolved, albeit gradually.

This case example illustrates three different patterns. The first (Fig. 4.16) shows very frequent cyclic seizures of the *regular flame* pattern, which become less frequent toward the end of the first 2-h window, with further reduction in seizure frequency in Fig. 4.17. The seizures stop approximately 24 min into Fig. 4.17. The spectrogram pattern then changes to a *broadband-monotonous* pattern and then finally *narrowband monotonous* by the third 2-h epoch (Fig. 4.18).

Case 9: (Figs. 4.19–4.20)

A 38-year-old man with alcoholic cirrhosis presented with variceal hemorrhage complicated by sepsis and renal failure, managed with ciprofloxacin and meropenem. He developed NCSE during his hospitalization. The cEEG showed seizures consisting of abrupt onset of beta activity every 2–5 min without clinical correlate.

This case example is illustrated across two consecutive 2-h epochs. In the first epoch (Fig. 4.19), there are *regular flame* seizures in a cyclic pattern that increase in frequency and ultimately fuse into a *broadband-monotonous* pattern, consistent with status epilepticus. The patient receives antiseizure medication, and the status epilepticus converts into a

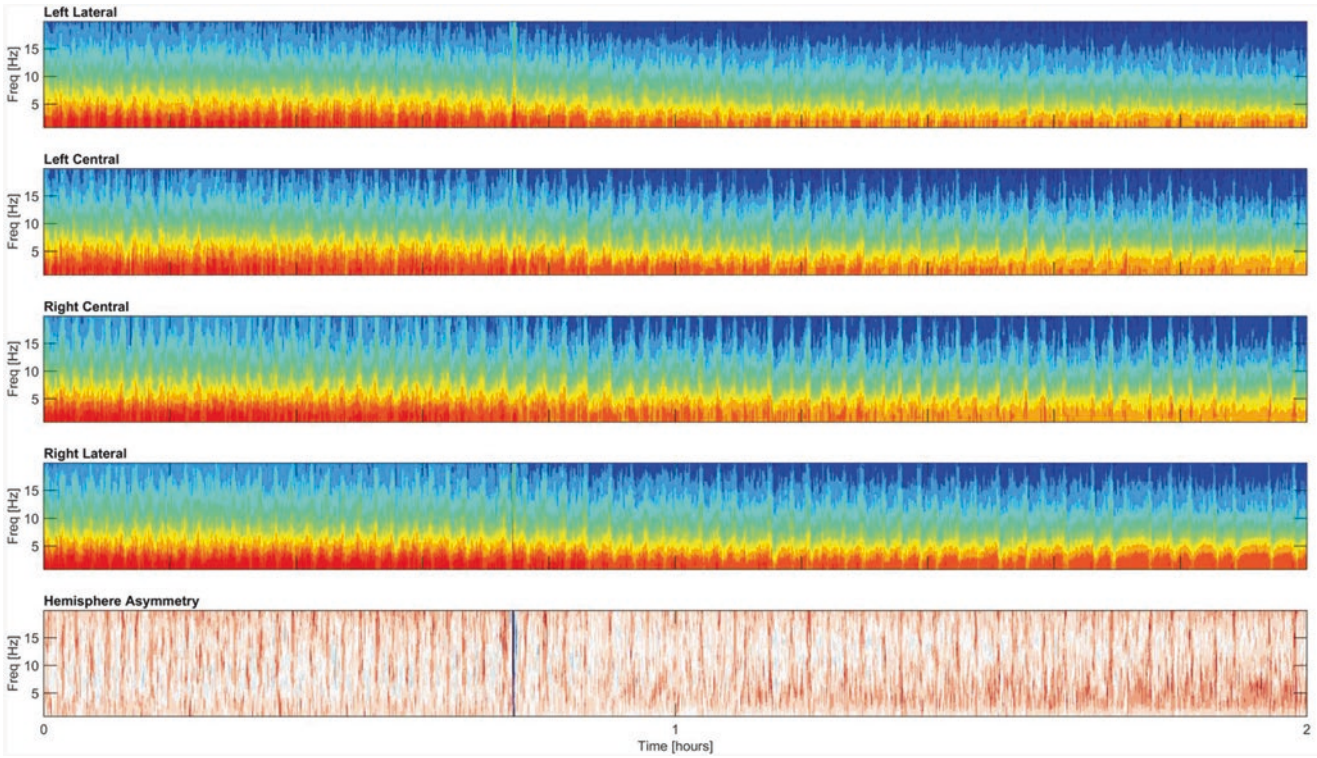

Fig. 4.16 Frequent *regular flame*-shaped seizures consistent with status epilepticus (Case 8)

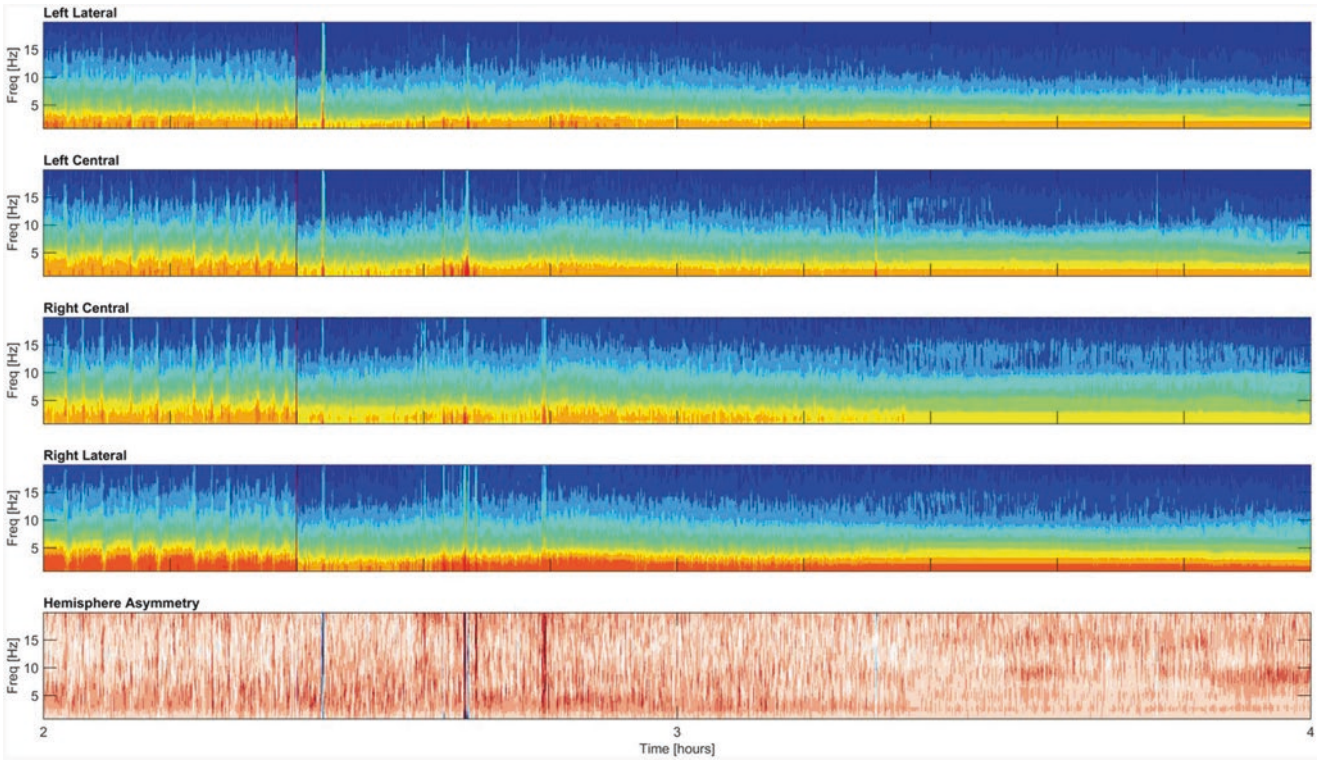

Fig. 4.17 Evolution of seizures as sedation increased (Case 8, continued). The CSA begins with *regular flame* seizures continued from Fig. 4.16, with a reduction in frequency followed by a transition to a *broadband-monotonous* pattern

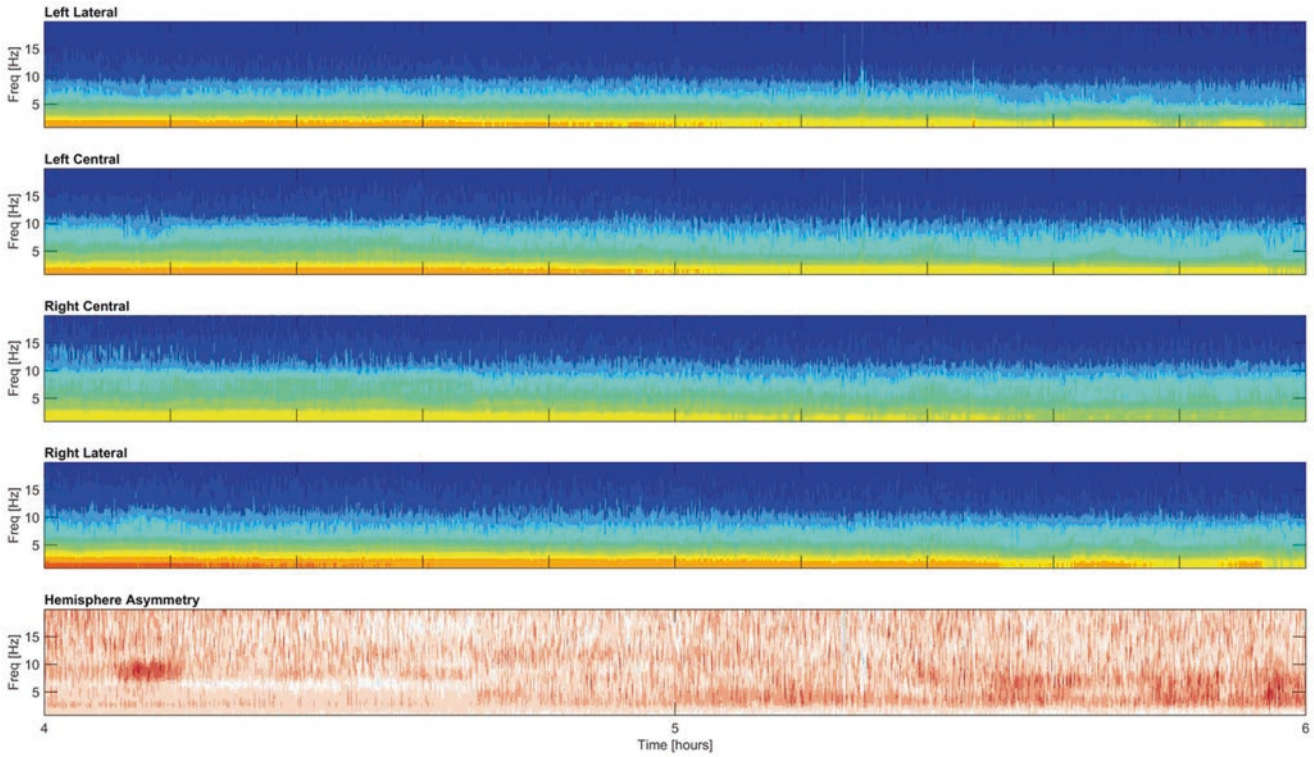

Fig. 4.18 Evolution to diffuse slowing (Case 8, continued). A continuation of Fig. 4.17, the CSA now shows a *narrowband-monotonous* pattern suggestive of diffuse slowing

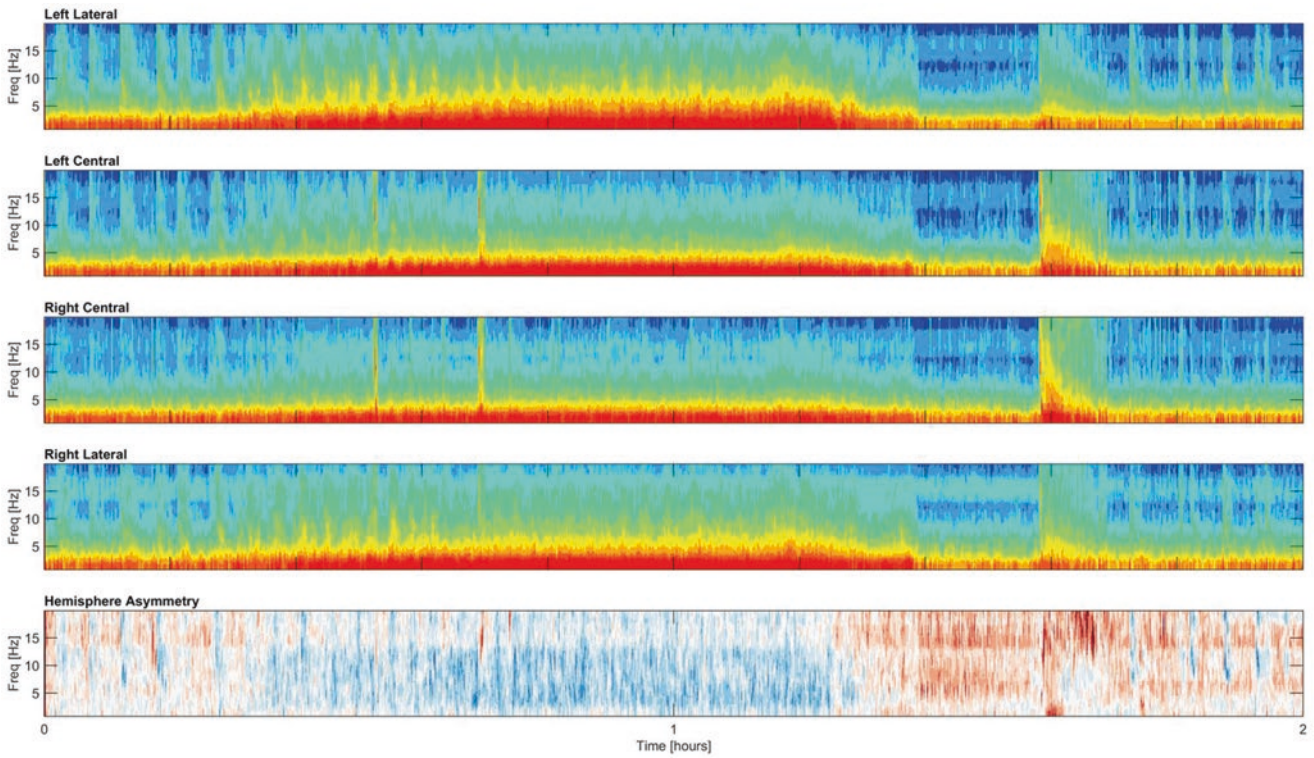

Fig. 4.19 *Regular flame* seizures evolving into *broadband-monotonous* status epilepticus (Case 9)

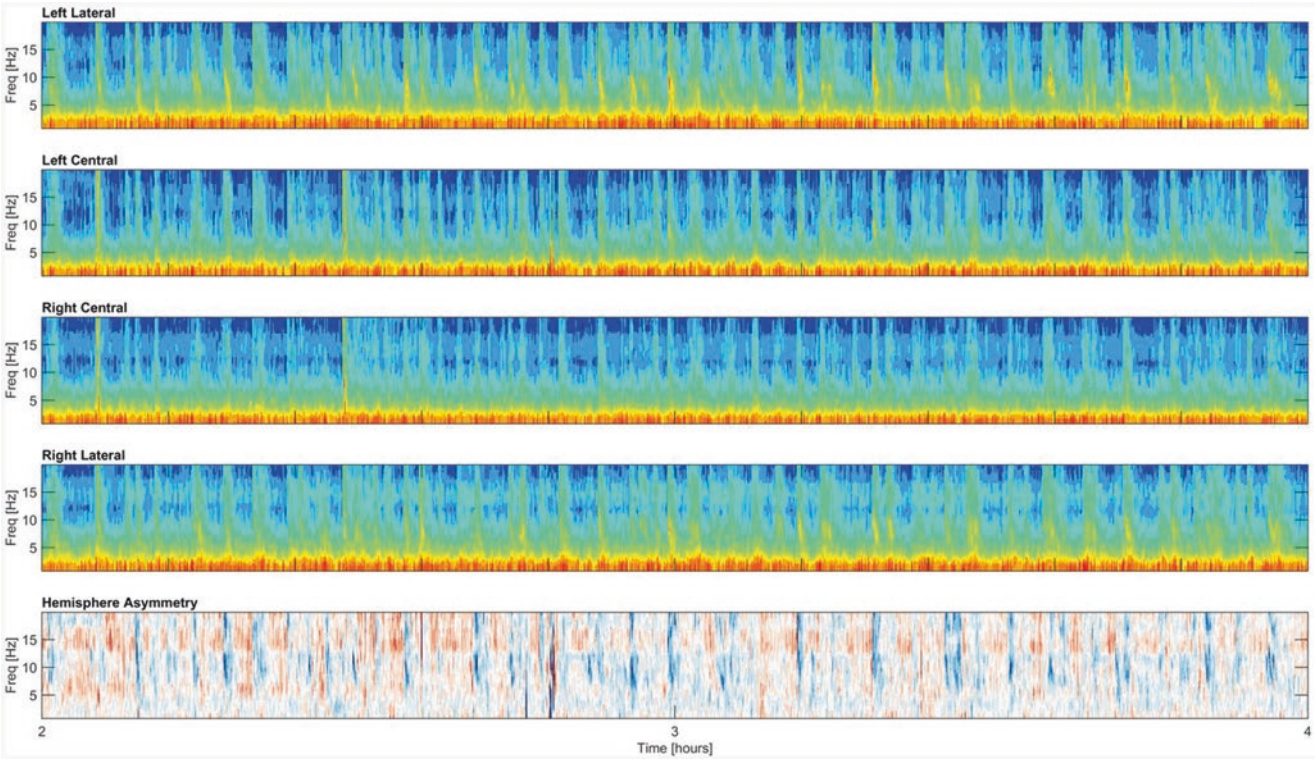

Fig. 4.20 Antiepileptic drug administration prompting the transition from status epilepticus back to *regular flame* seizures with a *narrowband-monotonous*, diffuse slowing background (Case 9, continued)

cyclic seizure pattern with less frequent *regular flame* seizures, on a *narrowband-monotonous* background pattern, corresponding to generalized slowing on the underlying EEG (Fig. 4.20).

Artifacts:

No qEEG method can escape the inherent limitations of scalp EEG and this is particularly true in the ICU environment. Frequent interventions and the use of multiple technologies make differentiating seizures and other patterns of interest from artifact sometimes challenging. We present a few examples to illustrate common artifacts seen on spectrograms in ICU patients.

Case 7, continued: (Fig. 4.21)

This spectrogram is from a later 2-h epoch of Case 7 (Figs. 4.14–4.15). Please refer back to Case 7 for the clinical vignette.

At the beginning of the epoch, the spectrogram shows a uniform deep blue, reflecting near-complete suppression of the EEG background. In this case the suppression is not due to pharmacological intervention, but rather reflects the end stage of severe diffuse anoxic brain injury. Near the end of the 2-h epoch, we see an abrupt change from very low to very high, full-bandwidth power, which manifests as a red color across the entire bandwidth of the spectrogram. This is a typical pattern for disconnection artifact. This pattern occurs when the EEG shows high-amplitude voltages due to amplifier saturation, due to either disconnection of the electrodes from the scalp or disconnection of all the electrodes from the headbox, as in this example.

Case 10: (Fig. 4.22)

A 51-year-old man presented with subarachnoid hemorrhage secondary to aneurysm rupture. An EEG was performed for vasospasm monitoring.

The background spectrographic pattern is intermediate between *narrowband* and *broadband monotonous*, raising the possibility of periodic discharges, although in this case in fact the background showed generalized high amplitude slowing. Interrupting this background pattern intermittently, one can see high-power red stripes that span the entire frequency range. Unlike the above example of disconnection artifact, these stripes are of much shorter duration suggesting very brief high-amplitude, high-frequency artifact such as is generated by movements leading to amplifier saturation or temporary EEG disconnection.

Case 11: (Fig. 4.23)

A 70-year-old man with a history of laryngeal cancer treated with radiation developed a delayed right common carotid artery rupture requiring carotid artery ligation. A cEEG was performed for cerebral perfusion monitoring in

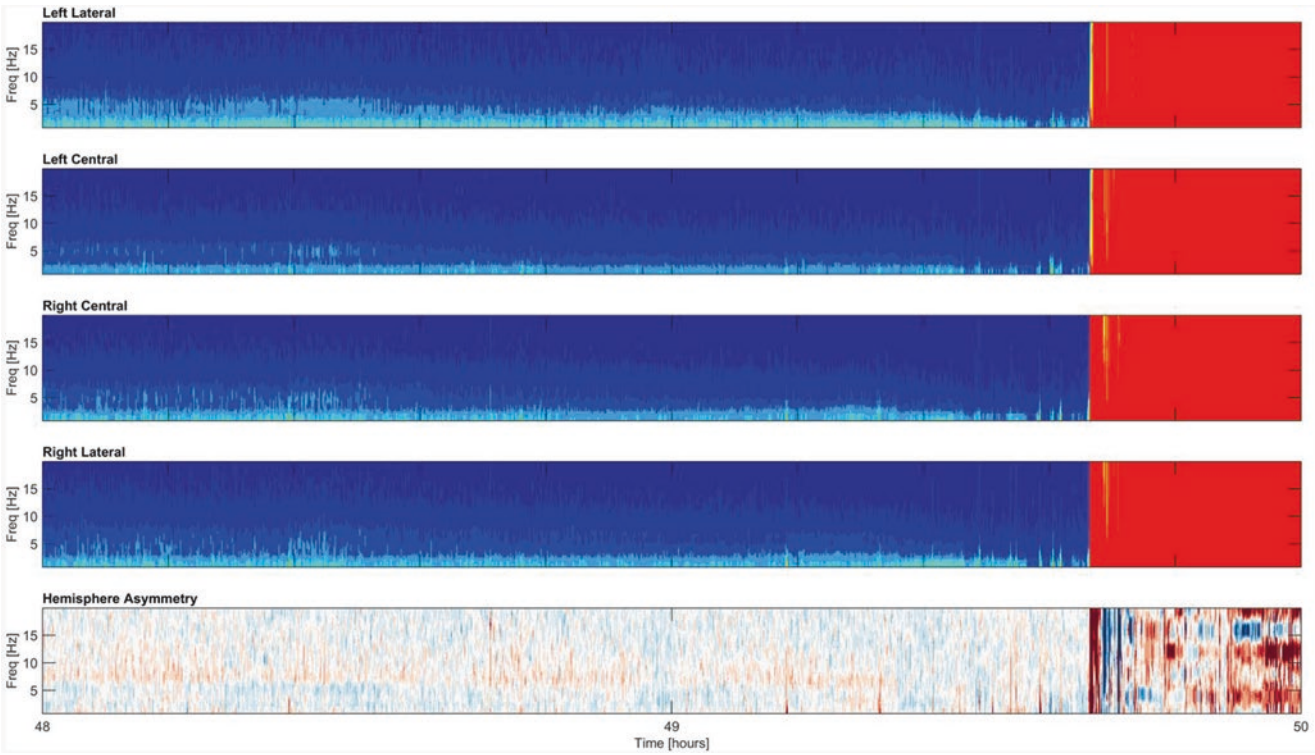

Fig. 4.21 Disconnection artifact (Case 7, continued). Seen as abrupt change in CSA from low power to sudden high-amplitude voltages due to amplifier saturation

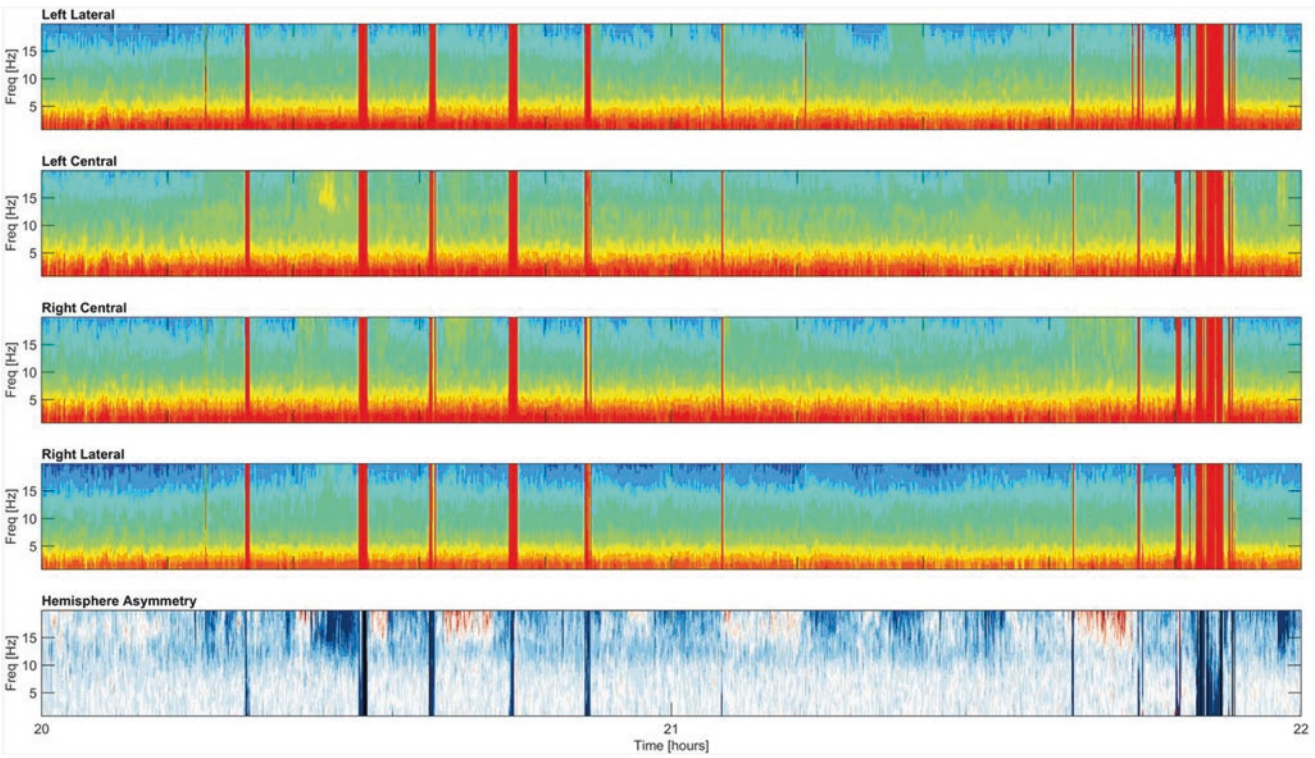

Fig. 4.22 Movement artifact (Case 10). High-amplitude, high-frequency artifacts of much briefer duration than those seen in disconnection artifact

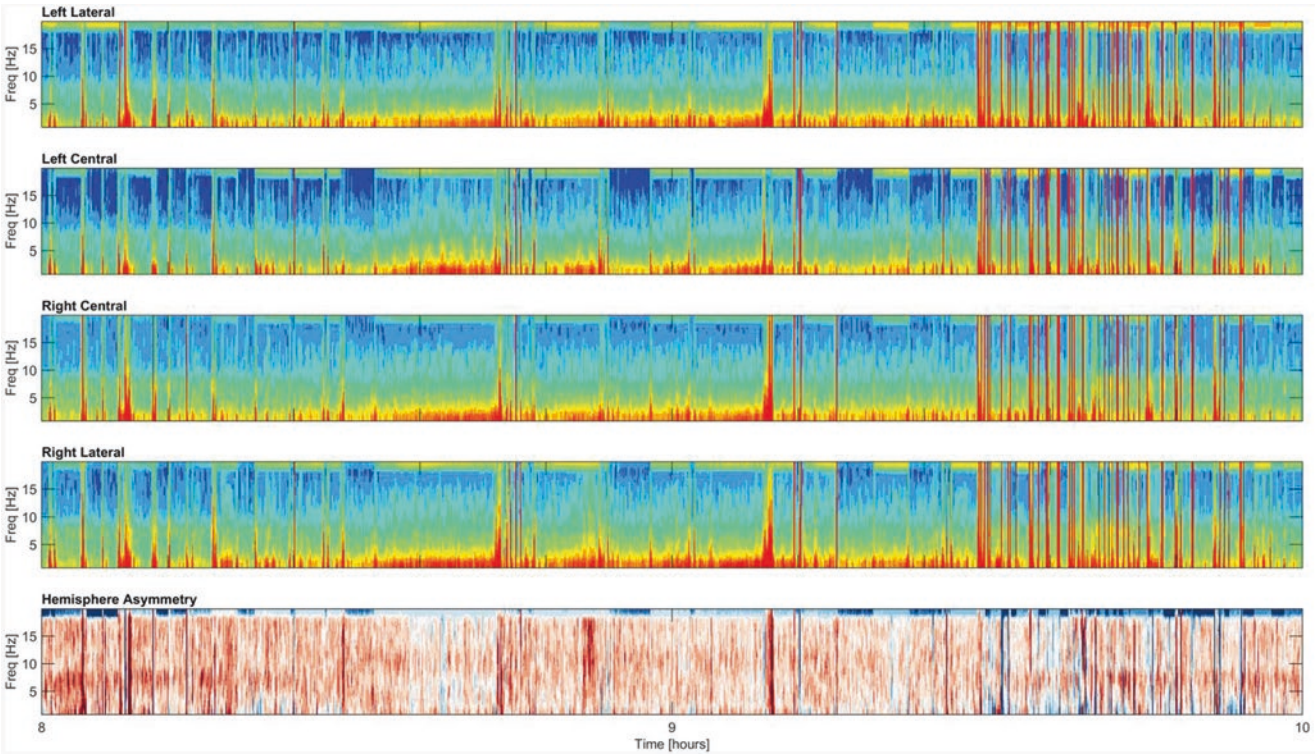

Fig. 4.23 Movement artifact (Case 11). Such artifacts can sometimes be mistaken for *regular flame* seizures

the setting of a drug-induced hypertension trial. There was no deterioration of neurological exam despite carotid ligation and withdrawal of hypertension-inducing medications. His EEG showed right frontotemporal slowing but no epileptiform discharges.

This spectrogram represents another typical example of frequent movement artifacts. One can imagine how the artifacts in the middle of the 2-h epoch might be mistaken for a *regular flame* pattern.

Case 6, continued: (Fig. 4.13)

On reexamination of the spectrogram in Fig. 4.13 from Case 6, in addition to the *narrowband-monotonous* pattern that constitutes the background, we note that there are transient bursts of yellow at higher frequencies. These events are sometimes described as looking like falling rain, rays of sunshine, or stalactites hanging from a cave ceiling. This pattern is typical of myogenic artifact. A similar myogenic artifact event is evident near the beginning of the epoch in Fig. 4.12, in the left lateral, right central, and right lateral regions.

There are many other types of artifacts that can give rise to unusual spectrogram patterns. For example, oscillating beds are characterized by the well-demarcated appearance of a high-power band that corresponds to the frequency at which the bed is oscillating. Electrical artifact at 55 Hz or 60 Hz caused by the numerous devices present in an ICU occurs at higher frequencies than are routinely displayed on spectrograms. Patient cleaning and repositioning may result in artifact that appears similar to the movement artifacts illustrated above. For patients undergoing active cooling following cardiac arrest, shivering – even minute shivering that is not clearly visible – can result in high-frequency movement and myogenic artifact. Some commercially available quantitative EEG software includes algorithms to identify and reduce artifact or to exclude leads with significant artifact from quantitative analysis and display.

Clinical Utility Of Quantitative EEG and Spectrograms

Determining the validity and utility of qEEG for clinical use is important to the continued use and optimization of these tools for patient care. Multiple studies have evaluated the sensitivity and specificity of various qEEG methods, though the most commonly evaluated has been spectrograms, usually by the terms CSA or DSA in the existing literature.

In a study of qEEG for pediatric ICU EEG data, one group compared the diagnostic accuracy of CSA and amplitude-integrated EEG for seizure identification [21]. For pediatric data, they found that sensitivity was relatively similar for CSA vs. aEEG (83 vs. 81%). However, overall, more seizures

were completely missed when using CSA (21%) vs. aEEG (14%). The most commonly missed seizures were those with low-amplitude, short and focal seizures. Other authors have also confirmed that CSA-guided review in many different protocols can support sensitive screening of critical pathological information in cEEG recordings [10, 12, 14, 21–25].

One study focusing on qEEG for interpretation of adult ICU EEG recordings concluded that spectrograms could be used as sensitive screening tool for seizures [11]. They trained two *non*-expert electrophysiology reviewers (neurology residents) to assess CSA signals for the presence or absence of seizures or other clinically important patterns. The reviewers were blinded to the presence or absence of seizures and were not allowed to view the primary cEEG data. An independent experienced electroencephalographer reviewed the raw EEG within 60 s on either side of each mark and recorded any seizures. Seizures were considered to have been detected if the CSA mark was within 60 s of the seizure. The CSA reviewers in this study achieved high seizure detection rates, but the study design deliberately allowed high false-positive rates to do so.

In a follow-up study, by allowing reviewers to review selected segments of raw cEEG data when guided by CSA-based screening (see Fig. 4.1), the authors hypothesized that the time required for review would be significantly less than required for conventional review of the entire raw cEEG without compromising the sensitivity for seizures or other critical pathologies [10]. This method also mirrors the way spectrograms are typically used in actual clinical practice by EEG experts, i.e., as an addition and aid for reviewing the raw EEG. In this study CSA-guided cEEG review identified all patients with seizures and detected 87% of all individual seizures among the cohort. Using this method, they were also able to detect period epileptiform discharges, rhythmic delta activity, focal slowing, and generalized slowing in >95% of patients. Using this method, they found CSA-guided screening identified the vast majority of seizures and other abnormal patterns while cutting review times by nearly 75% and missing only rare, brief, highly localized, nonconvulsive seizures. The authors concluded that the correlation of CSA patterns with the underlying EEG was critical in achieving high sensitivity and efficiency.

Given that one of the major limitations of cEEG is the limited availability of expert neurophysiologists, it would be optimal if qEEG methods could be interpreted by a broader audience. Several groups have explored the possibility of training non-neurophysiologists to utilize qEEG trends for seizure detection. One group evaluated the diagnostic accuracy of electrographic seizure detection by neurophysiologists and non-neurophysiologists using qEEG trend panels. They found that in isolated review of a qEEG panel, there was an overall sensitivity of 84% and specificity of 69% for all reviewer types for the detection of the presence of seizures [26]. These results were corroborated by other groups that evaluated critical care nurses, residents, and fellows [27]. They found that accuracy was not different between nurses and physicians after a short training program. Amorim et al. favored challenging CSA displays, which included seizures (50%) and periodic discharges (35%), a much higher frequency than commonly seen in patients monitored in a neurological ICU [28]. The false-alarm rate for nurses in this study was twice as high as for epileptologists in cases involving periodic discharges without seizures. The false-alarm rate in CSA displays with periodic discharges was not systematically reported in other studies; however, the number of displays containing seizures was comparable (30–66%) [27–30]. These findings suggest that in cases in which separation of seizures from periodic discharges is challenging, non-expert review of CSA would likely benefit from combined CSA and raw EEG correlation by neurophysiologists, similarly to what was done in Moura's protocol [10].

Quantitative EEG Outside the Realm of Seizures

Quantitative ICU EEG also has clinical applications outside the realm of seizures and status epilepticus, particularly for ischemia detection. Delayed cerebral ischemia (DCI), a major complication that occurs after aneurysmal SAH, can be seen in up to 50% of patients [31, 32]. Currently, transcranial Doppler ultrasonography (TCD) to assess blood flow velocity in the major cerebral arteries is most commonly used, but is operator dependent and done at most once per day. cEEG can potentially provide continuous real-time data for DCI monitoring.

The two features of qEEG that are commonly used to detect ischemia are the alpha-delta ratio and the relative alpha variability [33]. As cerebral blood flow decreases, predominantly slower oscillations are seen in the EEG, and there is a sequential loss of alpha followed by delta frequencies and subsequent suppression [33]. The alpha-delta ratio (ADR) is the ratio of the sum of the power within the alpha band (8–13 Hz) and delta band (1–4 Hz). The ADR is typically displayed as a moving average or histogram. Figure 4.24 shows an example of how a relative drop in alpha frequency power compared to delta frequency power results in a decrease in the ADR. Foreman and Claassen showed changes in the ADR with changes in GCS, neurological exam, and treatment [33]. ADR was found to have a strong association with DCI in a retrospective study that looked at qEEG in 34 high-grade (Hunt and Hess IV and V) SAH patients with high sensitivity (100%) and relatively good specificity (76%) [34]. Relative alpha variability (RAV) is the other commonly used qEEG parameter to detect early ischemia. This method uses the alpha-to-total power ratio (8–12 vs. 1–20 Hz). One

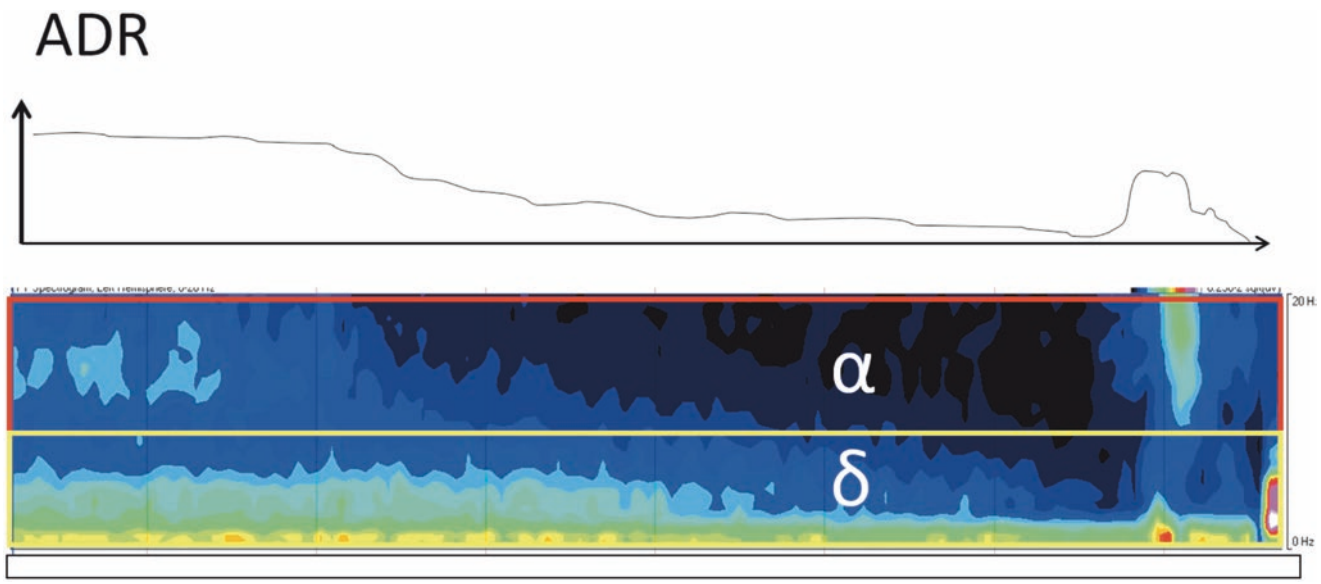

Fig. 4.24 Alpha-delta ratio (ADR). As the alpha power in a spectrogram decreases relative to delta frequency power, there is a decrease in the alpha-delta ratio

study evaluated RAV on a poor to excellent scale of 1–4, respectively [35]. A decrease in RAV by 1 in at least one channel was correlated risk of impending DCI.

Quantitative EEG is also increasingly used to help determine prognosis in post-cardiac arrest patients with anoxic brain injury. The burst suppression ratio, response entropy, state entropy, and wavelet sub-band entropy are some of the qEEG features that have been investigated in patients with anoxic brain injury [36]. The Cerebral Recovery Index (CRI) is a recently introduced prognostic index that combines power, Shannon entropy, alpha-to-delta ratio, "regularity," and coherence in the delta band. An initial pilot study found that higher CRI correlates with better outcomes [37].

Summary

qEEG can be a useful tool to augment evaluation of raw cEEG data in the ICU setting. Properly used, qEEG methods can reduce review time while maintaining adequate sensitivity. qEEG may reduce the burden of raw EEG review by expert encephalographers as well, since studies have shown that at least some qEEG trends can be evaluated by novices with minimal training to identify seizures and other patterns of interest. The increased employment of qEEG could potentially make tele-EEG review more feasible, thereby increasing the availability of EEG data at institutions which would not otherwise have these resources. Most importantly, the use of existing qEEG tools can facilitate real-time monitoring, which is vital to optimizing care of patients in the ICU setting.

There are still limitations with using existing qEEG technology that have proven challenging to overcome thus far. One of the most prominent limitations is that unlike EMU populations, seizures in critically ill patients frequently exhibit patterns of rhythmicity and evolution that are slower and may be harder to identify based on current algorithms [8]. Additionally, because of the variation in patterns seen in ICU patients, it is often difficult to have high expert interrater reliability in review of the raw EEG [38]. Thus, some of the limitations in sensitivities of qEEG methods may be related to this inherent inconsistency. There is also some concern that the false-positive rates for seizure identification are of concern as patients may be exposed to anticonvulsive therapy or anesthetics unnecessarily. Furthermore, some argue that these false-positive identifications may increase the burden of electroencephalographers to review the raw data and communicate misidentified events to the clinical providers. At present, it is still important to avoid using qEEG in isolation. Instead, it is best used as an adjunct to review of the raw EEG.

There are many directions in which qEEG can advance in the near future. A useful first step would be to develop standardized terminology with which to describe the most common physiologic and artifactual spectrogram patterns observed. By cataloging the common patterns and standardizing terminology, studies can better develop and cross-validate the sensitivity and specificity of these qEEG patterns to the raw EEG patterns. It may also help in the development of more uniform training modules for non-electrophysiology expert staff members who become involved in monitoring qEEG data at the bedside. In this

chapter, we introduced the use of some informal terminology (*regular flame*, *choppy flame*, *broadband monotonous*, *narrowband monotonous*) that could perhaps serve as a seed to develop such nomenclature.

Another important problem is determining the degree to which the information generated by qEEG (or EEG in general) impacts intervention and/or outcome in ICU patients. One of the main advantages of qEEG is the improved efficiency by which data can be reviewed. Does this or can this faster evaluation impact real-time clinical decision making? Are patients being clinically reexamined or scanned or receiving increased interventions based upon the information conveyed, and if so, does this lead to net benefit? A related topic is whether such efficiency can be improved by training a wider variety of staff members. The studies discussed above have shown that non-expert reviewers can be trained in evaluating qEEG with relatively preserved sensitivity. However, high false-positive rates remain problematic. Would this lead to overtreatment in certain cases? Alternatively, would the burden of cross-checking by neurophysiologists outweigh any benefit of training non-expert readers? Improved training programs for using qEEG technology will likely improve the clinical utility of qEEG, as will the development of a well-calibrated standardized terminology.

These issues are vital to the future of qEEG since these methods are meant to improve the delivery of care and hopefully patient outcomes. There has already been an exponential growth of interest in qEEG. This will likely continue as the field strives to improve qEEG algorithms and increase its integration into the real-time assessment of ICU patients.

References

1. Claassen J, Mayer SA, Kowalski RG, Emerson RG, Hirsch LJ. Detection of electrographic seizures with continuous EEG monitoring in critically ill patients. Neurology. 2004;62:1743–8.
2. Towne AR, Waterhouse EJ, Boggs JG, Garnett LK, Brown AJ, Smith JR, RJ DL. Prevalence of nonconvulsive status epilepticus in comatose patients. Neurology. 2000;54:340.
3. Claassen J, Vespa P. Electrophysiologic monitoring in acute brain injury. Neurocrit Care. 2014;21(Suppl. 2):S129–47.
4. Bassin S, Smith TL, Bleck TP. Clinical review: status epilepticus. Crit Care. 2002;6:137–42.
5. Niligan A, Shorvon S. Frequency and prognosis of convulsive status epilepticus of different causes: a systematic review. Arch Neurol. 2010;67:931–40.
6. Powers L, Shepard KM, Craft K. Payment reform and the changing landscape in medical practice: implications for neurologists. Neurol Clin Pract. 2012;2:224–30.
7. Sinha SR. Quantitative EEG basic principles. In: Handbook of ICU EEG monitoring; 2013. Demos Medical Publishing. New York, NY. p. 221–8.
8. Scheuer ML, Wilson SB. Data analysis for continuous eeg monitoring in the ICU: seeing the forest and the trees. J Clin Neurophysiol. 2004;21:353–78.
9. Laroche SM. Quantitative EEG for seizure detection. In:Handbook of ICU EEG monitoring. In; 2013. Demos Medical Publishing. New York, NY. p. 229–38.
10. Moura LMVR, Shafi MM, Ng M, Pati S, Cash SS, Cole AJ, Hoch DB, Rosenthal ES, Westover MB. Spectrogram screening of adult EEGs is sensitive and efficient. Neurology. 2014;83:56–64.
11. Williamson CA, Wahlster S, Shafi MM, Westover MB. Sensitivity of compressed spectral arrays for detecting seizures in acutely ill adults. Neurocrit Care. 2014;20:32–9.
12. Toet MC, van der Meij W, de Vries LS, Uiterwaal CSPM, van Huffelen KC. Comparison between simultaneously recorded amplitude integrated electroencephalogram (cerebral function monitor) and standard electroencephalogram in neonates. Pediatrics. 2002;109:772–9.
13. Prior PF, Virden RS, Maynard DE. An EEG device for monitoring seizure discharges. Epilepsia. 1973;14:367–72.
14. Abend NS, Dlugos D, Herman S. Neonatal seizure detection using multichannel display of envelope trend. Epilepsia. 2008;49:349–52.
15. Brandon Westover M, Shafi MM, Ching S, Chemali JJ, Purdon PL, Cash SS, Brown EN. Real-time segmentation of burst suppression patterns in critical care EEG monitoring. J Neurosci Methods. 2013;219:131–41.
16. Chemali J, Ching S, Purdon PL, Solt K, Brown EN. Burst suppression probability algorithms: state-space methods for tracking EEG burst suppression. J Neural Eng. 2013;10:056017.
17. Herta J, Koren J, Fürbass F, Hartmann M, Kluge T, Baumgartner C, Gruber A. Prospective assessment and validation of rhythmic and periodic pattern detection in NeuroTrend: a new approach for screening continuous EEG in the intensive care unit. Epilepsy Behav. 2015;49:273–9.
18. Thomson DJ. Spectrum estimation and harmonic analysis. Proc IEEE. 1982;70:1055–96.
19. Bokil H, Purpura K, Schoffelen JM, Thomson D, Mitra P. Comparing spectra and coherences for groups of unequal size. J Neurosci Methods. 2007;159:337–45.
20. Bokil H, Andrews P, Kulkarni JE, Mehta S, Mitra PP. Chronux: a platform for analyzing neural signals. J Neurosci Methods. 2010;192:146–51.
21. Stewart CP, Otsubo H, Ochi A, Sharma R, Hutchison JS, Hahn CD. Seizure identification in the ICU using quantitative EEG displays. Neurology. 2010;75:1501–8.
22. Shah DK, Mackay MT, Lavery S, Watson S, Harvey AS, Zempel J, Mathur A, Inder TE. Accuracy of bedside electroencephalographic monitoring in comparison with simultaneous continuous conventional electroencephalography for seizure detection in term infants. Pediatrics. 2008;121:1146–54.
23. Shellhaas RA, Soaita AI, Clancy RR. Sensitivity of amplitude-integrated electroencephalography for neonatal seizure detection. Pediatrics. 2007;120:770–7.
24. Rennie JM, Chorley G, Boylan GB, Presslet P, Nguyen Y, Hooper R. Non-expert use of the cerebral function motinor for neonatal seizure detection. Arch Dis Child Fetal Neonatal. 2004;89:37–41.
25. Bourez-Swart MD, van Rooij L, Rizzo C, de Vries LS, Toet MC, Gebbink TA, AGJ E, van Huffelen AC. Detection of subclinical electroencephalographic seizure patterns with multichannel amplitude-integrated EEG in full-term neonates. Clin Neurophysiol. 2009;120:1916–22.
26. Swisher CB, Shah D, Sinha SR, Husain AM. Baseline EEG Pattern on continuous ICU EEG monitoring and incidence of seizures. J Clin Neurophysiol. 2015;32:147–51.
27. Dericioglu N, Yetim E, Bas DF, Bilgen N, Caglar G, Arsava EM, Topcuoglu MA. Non-expert use of quantitative EEG displays for seizure identification in the adult neuro-intensive care unit. Epilepsy Res. 2015;109:48–56.
28. Amorim E, Williamson CA, Moura LMVR, Shafi MM, Gaspard N, Rosenthal ES, Guanci MM, Rajajee V, Westover MB. Performance

of spectrogram-based seizure identification of adult EEGs by critical care nurses and neurophysiologists. J Clin Neurophysiol. 2016:1. doi:10.1097/wnp.0000000000000368.
29. Topjian AA, Fry M, Jawad AF, Herman ST, Nadkarni VM, Ichord R, Berg RA, Dlugos DJ, Abend NS. Detection of electrographic seizures by critical care providers using color density spectral array after cardiac arrest is feasible. Pediatr Crit Care Med. 2015;16:461–7.
30. Swisher CB, White CR, Mace BE, Dombrowski KE, Husain AM, Kolls BJ, Radtke RR, Tran TT, Sinha SR. Diagnostic accuracy of electrographic seizure detection by neurophysiologists and non-neurophysiologists in the adult ICU using a panel of quantitative EEG trends. J Clin Neurophysiol. 2015;32:324–30.
31. Claassen J, Bernardini GL, Kreiter K, Bates J, Du YE, Copeland D, Connolly ES, Mayer SA. Effect of cisternal and ventricular blood on risk of delayed cerebral ischemia after subarachnoid hemorrhage: the Fisher scale revisited. Stroke. 2001;32:2012–20.
32. Roos YB, de Haan RJ, Beenen LF, Groen RJ, Albrecht KW, Vermeulen M. Complications and outcome in patients with aneurysmal subarachnoid haemorrhage: a prospective hospital based cohort study in The Netherlands. J Neurol Neurosurg Psychiatry. 2000;68:337–41.
33. Foreman B, Claassen J. Quantitative EEG for the detection of brain ischemia. Crit Care. 2012;16:216.
34. Claassen J, Hirsch LJ, Kreiter KT, Du EY, Connolly ES, Emerson RG, Mayer SA. Quantitative continuous EEG for detecting delayed cerebral ischemia in patients with poor-grade subarachnoid hemorrhage. Clin Neurophysiol. 2004;115:2699–710.
35. Vespa PM, Nuwer MR, Juhász C, Alexander M, Nenov V, Martin N, Becker DP. Early detection of vasospasm after acute subarachnoid hemorrhage using continuous EEG ICU monitoring. Electroencephalogr Clin Neurophysiol. 1997;103:607–15.
36. Wennervirta JE, Ermes MJ, Tiainen SM, et al. Hypothermia-treated cardiac arrest patients with good neurological outcome differ early in quantitative variables of EEG suppression and epileptiform activity. Crit Care Med. 2009;37:2427–35.
37. Tjepkema-Cloostermans MC, van Meulen FB, Meinsma G, van Putten MJAM. A Cerebral Recovery Index (CRI) for early prognosis in patients after cardiac arrest. Crit Care. 2013;17:R252.
38. Jirsch J. Computer-assisted interpretation of EEG for the ICU: monitoring made palatable. Clin Neurophysiol. 2011;122:1901–3.